12-19-2003

Luminescent Semiconductor Quantum Dots (QDs) and Their Nanoassemblies as Bioprobes

Yongfen Chen
University of New Orleans

LUMINESCENT SEMICONDUCTOR QUANTUM DOTS (QDs) AND THEIR NANOASSEMBLIES AS BIOPROBES

A Dissertation

Submitted to the Graduate faculty of the
University of New Orleans
in partial fulfillment of the
requirements for the Degree of

Doctor of Philosophy
in
The Department of Chemistry

by

Yongfen Chen

B.E., Eastchina Institute of Chemical Technology, 1989
M.S., Eastchina Institute of Chemical Technology, 1994

ACKNOWLEDGMENTS

This dissertation is dedicated to my wife Zhen Ling and my son Shidong Chen. Without their love, encouragement, help and understanding, it would not be possible for me to complete my Ph.D studies.

I would like to thank my research advisor Professor Zeev Rosenzweig for the generous support of my research work for the past four years and for his continuous advices, helpful discussions and suggestions.

I would like to thank my advisory committee members Professor Matthew A. Tarr, Professor John B. Wiley, Professor Ron Evilia, Professor Kevin Stokes and Professor Scott L. Whittenburg for their advices and suggestions during my research work.

I would like to thank everyone in our research group for your cooperation and kindness. The time I spent with you will be remembered.

TABLE OF CONTENTS

LIST OF FIGURES

ABSTRACT

Quantum dots (QDs) CdS and CdSe were synthesized in three different media including reverse micelles, aqueous solution, and trioctylphosphine oxide/trioctylphosphine (TOPO/TOP). Transmission electron microscope (TEM), X-ray diffraction (XRD), UV-VIS, fluorescence spectroscopy and microscopy were used to characterize the QDs and their nanoassemblies. CdS QDs synthesized in reverse micelles showed broad emission spectra. CdSe-CdS QDs with core shell structure synthesized in aqueous solution showed more than 30% emission quantum yield. CdSe-CdS QDs of different emission colors were prepared. CdSe and CdSe-ZnS QDs were also synthesized in TOPO/TOP media. This synthesis route produced highly luminescent CdSe QDs with over 50% emission quantum yield.

The application of QDs as ions probes and methods to encapsulate QDs in nanospheres including micelles, glyconanospheres and silica nanospheres and the use of these nanospheres in bioassays are described. CdS QDs capped with different ligands such as thioglycerol, cysteine and polyphosphate showed different responses to biological relevant ions. The emission intensity of polyphosphate capped CdS QDs was affected by all the tested ions and did not show a selective response. On the other hand, the emission of thioglycerol capped CdS QDs was selectively quenched by copper ions while the emission of cysteine capped CdS QDs was selectively enhanced by zinc ions. Stern-Volmer equation was applied to correlate the emission intensity of the CdS QDs and the copper ion concentration. A Lagmuir isotherm binding equation was used

to describe the relation between the emission intensity of cysteine capped CdS QDs and zinc ion concentration. The possible mechanism to explain the effects of capping ligands on CdS QDs responses to ions is also discussed. CdSe QDs synthesized in TOPO/TOP media were encapsulated in nanospheres for bioassay applications. The glyconanospheres contained a large number of glucose residues on their surface and showed high binding activity towards the lectinic protein Concanavalin A (Con A). Silica nanospheres containing hundreds of CdSe QDs were functionalized with thiol groups to enable the conjugation of streptavidin to the nanospheres. The streptavidin modified silica nanospheres were used as luminescent indicators in a sandwich immunoassay for the detection of antiprotein A antibody. The advantages and disadvantages of the nanospheres based bioassay are discussed.

CHAPTER ONE: INTRODUCTION

1.1 Nanomaterials

Nanomaterials have attracted tremendous research interest in both academic institutions and industry. They have been used in clinical diagnostics (1-3), catalysis (4-9), drug delivery (10-13), and optical and mechanical devices (14-17). To develop these applications it is important to investigate how the optical, magnetic and mechanical properties of nanomaterials differ from that of bulk materials and molecules or atoms. As the particles' size approaches nanometric dimensions, materials often show different properties that are only found in this size region. Although nanoscience and nanotechnology are a new scientific discipline, nanomaterials themselves are not new. For example Zinc and Cadmium sulfides and selenides were used to dope glasses to produce yellow, orange and red color glasses more than one hundred years ago. These colored glasses contained semiconductor nanoparticles (18). In biological systems, proteins, DNA, chromosomes and most viruses are all in the nanometer scale (19).

1.2 Quantum Dots (QDs)

1.2.1 Size dependence of the band gap energy of QDs

Semiconductor QDs are inorganic nanoparticles that contain hundreds to several thousands of atoms (20). When the size of semiconductor nanocrystals is smaller than the Bohr radius of the excited electron-hole pair, quantum confinement effect occurs and the band gap energy starts to increase with the decrease of particle size. For example, the Bohr radius of CdS QDs is about

3 nm (~3000 to ~ 4000 atoms). When the diameter of CdS nanocrystals is comparable or smaller than 6 nm, the band gap energy of CdS increases, which can be observed as a blue-shift in the absorption threshold (21). Figure 1.1 illustrates the quantum confinement effect on the band gap energy of QDs.

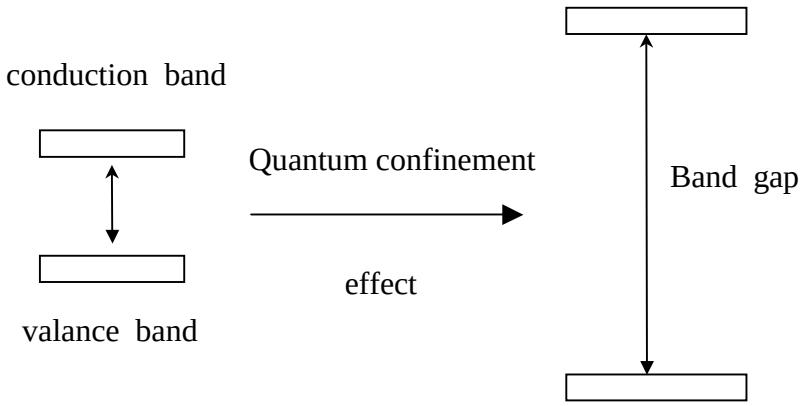

Fig. 1.1 Size dependence of the band gap of semiconductor QDs

1.2.2 Optical properties of QDs

Recent advances in the synthesis techniques enable researchers to prepare high crystallinity QDs with controlled size distribution. The size of CdSe QDs is tunable from 2 nm to 8 nm with a standard deviation less than 5% (22). When irradiating semiconductor QDs with visible light or UV light, the electrons in the valence band are excited to the conduction band. The relaxation of the excited electrons back to the ground state release the absorbed energy in the form of light. Therefore, semiconductor QDs are luminescent nanoparticles. The wavelength of emitted light is determined by the band gap energy. Since the band gap energy of the QDs is size dependent, the

emission color of the QDs is also size dependent. Figure 1.2 shows the size dependent emission of CdSe QDs. CdSe QDs averaging 3 nm in diameter emit green light. On the other hand, 6 nm QDs have smaller band gap, and therefore emit red light. The tunable emission properties of QDs are unique. In contrast organic dyes do not show such tunability.

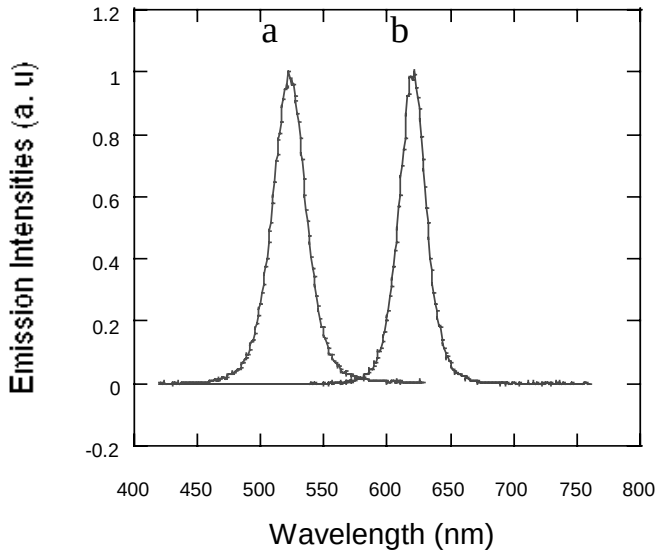

Fig. 1. 2 Emission spectra of CdSe QDs when excited at 400 nm. curve (a) 3 nm QDs; curve (b) 6 nm QDs.

In addition, QDs have a very broad absorption spectrum that enable the excitation of a mixture of QDs of different emission colors with a single excitation wavelength. In contrast, organic dyes' absorption spectra are usually narrow. Therefore different excitation wavelengths are needed to excite each organic dye in a solution containing several dyes. Figure 1.3 A shows the absorption spectrum (curve a) and emission spectrum (curve b) of the organic dye fluorescein. Fluorescein shows a narrow absorption band and it can only be effectively excited at

a wavelength around 470 nm. Figure 1.3 B shows the absorption spectrum (curve a) and emission spectrum (curve b) of CdSe QDs. CdSe QDs have a very broad absorption spectrum that extends from 350 nm to 470 nm. Figure 3 also reveals that the emission spectrum of QDs is sharp and symmetric while the emission spectrum of fluorescein is broad and has a tail extending to long wavelengths. The tail often causes problems when a sample is labeled with multiple organic dyes due to the overlap of emission peaks.

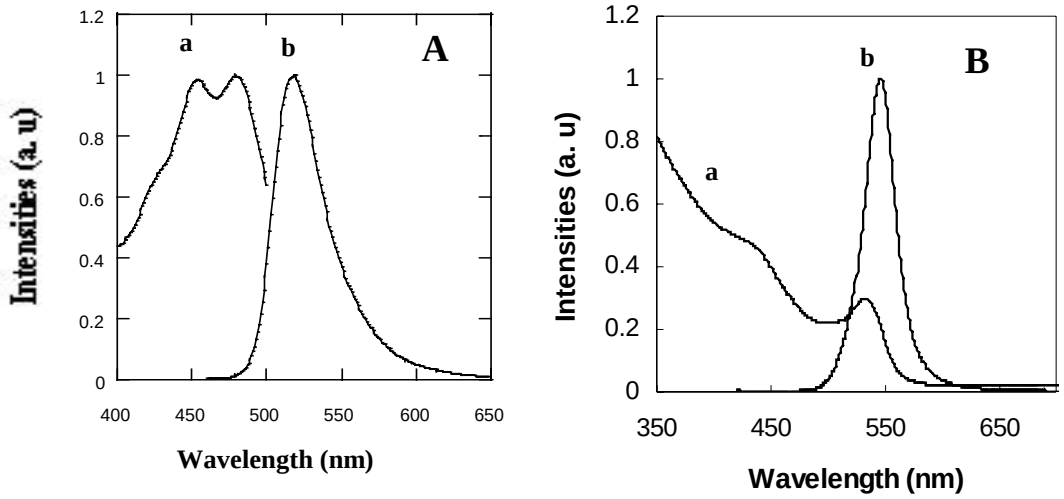

Fig. 1.3 Comparison of the absorption and emission spectra of fluorescein and QDs. (A) Fluorescein. Curve (a) shows the absorption spectrum; curve (b) shows the emission spectrum. (B) CdSe QDs synthesized in TOPO/TOP media. Curve (a) is the absorption spectrum. Curve (b) is the emission spectrum.

1.3 Preparation of QDs

1.3.1 Synthesis of CdS and CdSe QDs.

QDs have been synthesized in various media including aqueous solution, reverse micelles and TOPO/TOP. Aqueous solution provides a convinent medium for the synthesis of

nanoparticles (23-27). In this system the precursors for CdS or CdSe QDs are injected directly into water in the presence of a stabilizer such as sodium polyphosphate or other polymer to restrict the growth of the QDs. Herron et al. synthesized CdS QDs using thiophenolate as stabilizer (28). They prepared three stock solutions by dissolving cadmium acetate in methanol (stock solution A), sodim sulfide in 1:1 water-methanol solution (stock solution B) and thiophenol in methanol (stock solution C). They first mixed stock solution B and C, then added stock solution A. The CdS QDs formed immediately following the addition of cadmium acetate solution. CdS QDs could be collected as stable solids and redispersed in solution. They found that the size of the CdS QDs was controlled through varying the molar ratio of sodium sulfide to thiophenol (S/SPh). For example, when S/SPh was 0.5, the resulting CdS QDs were smaller than 1.5 nm in diameter. While when S/SPh was 4.5, the resulting CdS QDs were 3.5 nm in diameter. This is because thiophenol binds strongly to cadmium ions on the surface of the CdS QDs and limits their growth. Vossmeyer et al. (29) used 1-thioglycerol and sodium polyphosphate as stabilizers to synthesize CdS QDs. They first mixed $Cd(ClO_4)_2$ and the stabilzer in aqueous solution, then injected H_2S gas to the solution. The CdS QDs capped with thioglycerol were smaller than 2 nm in diameter while the QDs capped with sodium polyphosphate were from 5.8 nm to 9.6 nm in diameter as determined by X-ray diffractometry pattern. The high affinity of thioglycerol to surface cadmium ion of the CdS QDs led to smaller nanoparticles due to the inhibition of the CdS QDs growth. Swayambunathan et al. (30) developed a method to synthesize CdS QDs by radiolytic release of sulfide from thioglycerol in the presence of Cd^{2+} ions. In this study thioglycerol functioned as the S^{2-} ion source as well as a growth moderator. They found that the formation rate of CdS nanoparticles was strongly pH dependent due to the pH effect on the stability of Cd^{2+}/HS^- complex. At pH values from 4.0 to 5.3, the growth of the

CdS nanoparticles was controlled by the competition of thiolate ions with HS^- ions for the Cd^{2+} ions on the surface of the CdS nanoparticles. At neutral and basic solution, the growth of CdS nanoparticles was mainly due to the aggregation of cadmium-thiolate polynuclear complexes.

Reverse micelles (31-37) are another widely applied medium to synthesize semiconductor QDs. Reverse micelles are a water-in-oil heterogeneous system. Figure 1.4 is a sketch of the structure of reverse micelles used to synthesize CdS QDs.

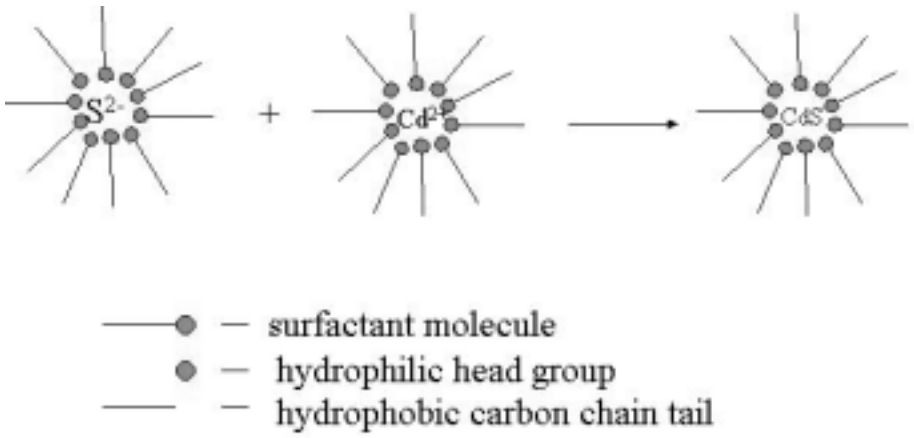

Fig. 1.4. The structure of reverse micelles containing S^{2-} and Cd^{2+} and CdS QDs

Water drops are stabilized in an organic phase by a surfactant with its hydrophilic head dissolved in the water pool and its hydrophobic tail in the oil phase. Towey et al (38) used a simple equation to correlate the water droplet size and w_o:

$$R/\text{ nm} = 0.18\, w_o + 1.5 \qquad (1)$$

R is the radius of the water droplet; w_o is the molar ration of water to surfactant (w_o = [Water]/[surfactant]). For a w_o =10 reverse micelle solution, the diameter of water droplet is about 6.6 nm. Therefore the size of the water drops can be adjusted by simply changing the ratio of water to surfactant concentration w_o. Generally, high w_o means larger water pool, which leads to the formation of larger nanoparticles. However, other processes such as Ostwald ripening and flocculation complicate the growth of nanoparticles in reverse micelles. Lianos et al. (39) used bis(2-ethylhexyl) sulfosuccinate sodium salt (Aerosol OT, AOT) reverse micelle of $w_o = 5$ and 32 respectively to synthesize CdS QDs. The luminescence of CdS QDs synthesized in reverse micelle solution at $w_o = 5$ had a peak at 470 nm. The emission spectrum of CdS QDs synthesized at $w_o = 32$ had a peak at 650 nm due to large particle size. This observation confirmed that high value of w_o produced large particles. CdSe QDs were also prepared in AOT reverse micelles. Steigerwald et al.(40) prepared CdSe QDs by injecting bis(trimethylsilyl) selenium [$Se(TMS)_2$], which was used as Se precursor to an AOT reverse micelle solution containing Cadmium ions. Do et al (41) found that the organometallic molecule $Se(TMS)_2$ decomposes in aqueous solution and releases Se^{2-} ions. Steigerwald et al. synthesized CdSe QDs in three reverse micelle solutions with w_o = 5.4, 2.7, and near nero respectively. They found the absorption threshold of CdSe QDs shifted from 600 nm to 470 nm when the w_0 changed from 5.4 to near zero. Based on the relation of absorption threshold and the QDs size (42), CdSe QDs synthesized in reverse micelle solution at w_0=5.4 was larger than that synthesized at w_0 near zero. Transmission electron microscope (TEM) images revealed that the size of CdSe synthesized in reverse micelles with w_0 near 0 was about 1.7 nm in diameter while CdSe QDs prepared in reverse micelle solution with w_0 = 5.4 were 4.5 nm in diameter.

Thermolysis of organometallic precursors in TOP/TOPO media is one of the most extensively applied methods for the synthesis of CdS and CdSe QDs (43-47). In 1993, Murray et al. (48) developed a novel method to prepare CdS, CdSe and CdTe QDs by injecting $Cd(CH_3)_2$ and $SE(TMS)_2$ dissolved in TOP solution to hot TOPO media (SE= S, Se, and Te.). By varying the molar ratio of $Cd(CH_3)_2$ to $Se(TMS)_2$, they were able to tune the sizes of CdSe QDs from 1.5 nm to 10 nm in diameter with a standard deviation of less than 4%. CdSe QDs showed a quantum yield as high as 20% at room temperature. However, the organometallic precursor $Cd(CH_3)_2$ is highly toxic and sensitive to moisture and air. As a result, the synthesis of CdSe QDs needs to be conducted in a dry-box with high caution. To overcome this problem, Peng et al. developed a greener route to synthesize CdSe QDs (49-51). They found CdO, $Cd(Ac)_2$ and $CdCO_3$ could be used to replace $Cd(CH_3)_2$ as cadmium precursors. These compounds were stable and safe compared to the previously used organometallic precursors. Using these safe precursors, they were able to synthesize CdSe QDs ranging from about 1.5 nm to 25 nm in diameter. Without any size selective precipitation, the standard deviation in the diameter of QDs smaller than 15 nm was between 5 to 10%. The CdSe QDs synthesized by this greener route had up to 80% emission quantum yield. This greener route provided a safe and simple method to synthesize high quality CdSe QDs. Recently Pradhan et al. (52) used a single precursor to prepare CdS QDs. They first prepared cadmium-alkylxanthates salt ($Cd\text{-}R\text{-}CH_2\text{-}CH_2\text{-}OCS_2^-$). This salt is air-stable. Heating this metal alkylxanthate salt in hexadecylamine (HAD) at 70˚C produced high quality, nearly monodisperse CdS QDs with a narrow emission peak at 450nm. The advantage of this synthesis technique is that the reaction was carried out in a test tube without any air sensitive techniques. The size of the CdS QDs was controlled by varying the heating temperature. For example, CdS QDs averaged 5.2 nm in diameter when the precursor

was heated at 90˚C while the size of CdS QDs was 3.5 nm when the single precursor was heated at 70˚C. Besides the methods introduced above, other media such as phospholipid vesicles (53-54), polymer films (55-57), cavities of zeolites (58), interlayer spaces of clays (59), pulse radiolysis (60-61) and sol-gel systems(62) have also been used to prepare QDs. In these media, the growth of QDs is restricted either by a stabilizer or by using a solid nanometric reactor. QDs synthesized in solid media such as polymer film, pores of zeolites, clays, and sol-gels were trapped in these media and were not available for further surface modification for use in solution based applications. In this dissertation, the first three media of aqueous solution, reverse micelles and TOPO/TOP were applied to synthesize CdS and CdSe QDs.

1.3.2 Synthesis of core-shell QDs

QDs contain hundreds to thousands of atoms. These atoms are mostly located on the surface of the QDs. For example, for a 1 nm QD nearly 100% of the atoms are surface atoms. The surface atoms are not fully coordinated and are highly reactive. They also form surface defects (63). Surface defects often decrease the emission efficiency of QDs. To remove such defects, organic molecules have been used to ‘cap’ QDs. QDs capped with organic molecule show near 10% emission quantum yield (64-65). This is attributed to the fact that organic ligands can only cap cationic or anionic surface sites, and the capping is never complete. Several research groups introduced methods to prepare core shell QDs where a shell material of a larger band gap energy coats the core particles. In core-shell QDs, the cores are separated from the environment and changes in QDs environment have only a minor effect on their optical properties. Sphanhel et al. (66) synthesized CdS QDs in aqueous solution using sodium hexametaphosphate as a stabilizer. The prepared CdS QDs had less than 1% emission efficiency

and broad emission band extending from 500 and 700 nm. After formation of a $Cd(OH)_2$ shell on the surface of CdS QDs by dropwisely addition of NaOH and $Cd(ClO_4)_2$ solution, the emission efficiency of CdS-$Cd(OH)_2$ QDs increased dramatically to above 50%. The activated CdS QDs showed very narrow emission band between 460 nm and 530 nm. Hines et al. (67) developed a method to cap CdSe QDs with a ZnS shell by a two-step single flask method. The CdSe QDs were synthesized using the method reported by Murray et al. in TOPO/TOP media (64). Then the mixture of diethyl zinc and $(TMS)_2S$ was injected into the CdSe QDs-TOPO solution at 300ºC. The emission quantum yield of ZnS capped CdSe QDs was as high as 50%. Using this method, Dabbousi and coworkers (68) investigated the influence of ZnS shell thickness on the emission efficiency of CdSe QDs. They prepared CdSe QDs with a ZnS shell of 0, 1.3, 2.6 and 5.3 monolayers, they found 1.3 monolayer of ZnS shell provided the highest emission efficiency of 50% while the bare CdSe QDs had only 15% emission efficiency. They ascribed the low emission efficiency of CdSe QDs with a thick ZnS shell to the formation of nonradiative recombination sites in thick ZnS shell. Li et al. (69)developed an epitaxial method to grow CdS shell on the surface of CdSe core through successive ion layer adsorption and reaction (SLIAR) method. The CdSe core was synthesized using the greener route as introduced above(49). CdO dissolved in oleic acid and 1-octadecene(ODE) and sulfur dissolved in ODE solution were used as precursors for the growth of CdS shell. These precursors were injected alternatively with tight quantity control to the CdSe core solution at 240ºC. They found that CdSe core maintained their narrow size distribution and sharp emission spectra after the formation of CdS shell of five monolayers. The emission quantum yield of CdSe-CdS core shell nanocrystals ranged from 20% to 40%. The CdSe-CdS QDs showed superior processibility to corresponding CdSe core. The CdSe-CdS QDs maintained their emission quantum yield after precipitation or extraction

purification procedures, while the bare luminescent CdSe QDs were almost extinguished after a similar precipitation procedure. Recently, Mekis et al. (70) developed a unique procedure to synthesize CdSe-CdS core-shell nanocrystals. The CdSe core was synthesized by injection the cadmium stock solution ($Cd(Ac)_2$ dissolved in TOP) to hot TOPO solution containing Se-TOP at 300ºC. They found that injection of H_2S gas into CdSe core solution at 140Cº dramatically increased the emission quantum yield of CdSe QDs to 85%. The increase of emission quantum yield was attributed to the formation of a CdS shell on the surface of CdSe core. Since in CdSe core solution there was unreacted $Cd(Ac)_2$, it reacted with H_2S gas and formed a CdS shell. Pradhan et al. (52) used single precursor of cadmium hexadecyl xanthates (HDX) salt to prepare CdS QDs in hexadecylamine media at 70˚C. The CdS QDs were capped with a ZnS shell by heating zinc-HDX salt at the same temperature. The formation of a ZnS shell was manifested by a 7-fold increase of the quantum yield of the CdS QDs from about 2% to 13.9%. Malik et al. (71) prepared CdSe-CdS, CdSe-ZnS CdSe-ZnSe core shell QDs by heating a single source precursor of bis(hexyl(methyldithio-/selenocarbomato) cadmium/zinc in TOPO media at 250˚C . The synthesized core shell QDs showed band edge emission. However the emission spectra were relatively broader compared to the core shell CdSe-ZnS QDs synthesized by Hines et al.(67).

1.3.3 Surface modification of QDs.

CdSe QDs synthesized in TOPO/TOP media were capped with surfactant molecules and they were only dispersible in organic solvents. Hydrophilic ligands containing thiol group were used to exchange the surface bound surfactant and make the CdSe QDs water-soluble. Aldana et al. (72) successfully capped CdSe QDs with a series of ligands including mercaptoacetic acid, mercaptobenaoic acid, mercaptopropionic acid, 11-mercaptoundecanoic acid, dihydrolipoic acid,

and 1,4-dithio-D,L-threitol. The ligand exchange reaction was conducted by refluxing the mixture of CdSe QDs capped with TOPO and the ligands in methanol solution at 65ºC overnight. The ligand capped CdSe QDs were highly water-soluble. Merccaptoacetic acid capped CdSe QDs were negatively charged, they could interact with positively charged polymer through electrostatic interaction. Potapova et al. (73) demonstrated that an amphiphilic positively charged polymer ligands transferred mercaptoacetic acid capped CdSe QDs from aqueous solution to chloroform phase due to adsorption of polymer on their surfaces. Wang et al.(74) used a series of hydrophilic organic dentrons with thiol group at the focal point to modify the surface of CdSe QDs through refluxing the mixture of CdSe QDs capped with TOPO and dentron in methanol solution. Dentrons capped CdSe QDs showed higher photochemical stability (under UV radiation) compared to CdSe QDs capped with linear ligands. Ligands capped water-soluble CdSe QDs could be used to conjugate biomolecules in bioanalysis applications.

1.4 Applications of QDs

QDs were used as luminescent biological labels. In 1998, Chan et al (75) modified CdSe-ZnS QDs with a protein transferrin and used them to label HeLa cells through receptor-mediated endocytosis. Their results showed that the attached transferring molecules were still active and were recognized by the receptors on the cell surface. They also demonstrated that when QDs labeled with IgG incubated with bovine serum albumin (BSA) and a specific polyclonal antibody, the polyclonal antibody recognized the Fab fragments of IgG and induced an extensive aggregation of CdSe-ZnS QDs. Weiss et al (76) used silica coated CdSe-ZnS QDs with green and red emission colors to label mouse fibroblasts. QDs covalently labeled with biotin was used to label fibroblasts, which were previously incubated in phalloidin-biotin and streptavidin.

The green and red labels were clearly spectrally resolved. Rosenthal et al (77) used ligands-conjugated QDs to target cell surface receptors, ion channels and transporters. They showed that QDs labeled with the neurotransmitter serotonin interacted with antidepressant-sensitive, human and Drosophila serotonin transporters (hSERT, dSERT) that were expressed in HeLa and HEK-293 cells. They found that serotonin labeled QDs dose-dependently inhibited the transport of radiolabeled serotonin, with an estimated half-maximal activity (EC50) of 33×10^{-6} M (dSERT) and 99×10^{-6} M (hSERT). Their results showed the possibility of using ligand-conjugated luminescent nanocrystals as versatile probes of cell membrane proteins in living cells. Akerman et al. (78) used peptide coated QDs as luminescent probes *in vivo*. QDs coated with peptides could specifically target mice's lung, blood vessels and lymphatic vessels in tumors. QDs were also used in multiphoton fluorescence microscopy in living animals. Larson et al. (79) visualized QDs through the skin of living mice as deep as hundreds of micrometers. To increase biocompatibility, Dubertret et al. (80) encapsulated single QDs in phospholipid block-copolymer micelles. These QDs doped micelles were used as luminescent labels in *in vitro* and *in vivo* studies. When injected into Xenopus embryos, the QDs containing micelles were stable, nontoxic, slow to photobleach and cell autonomous. Wu et al. (81) demonstrated the advantages of QDs as an alternative to organic dyes in biolabeling studies *in vivo*. In their study QDs were modified with IgG and streptavidin to label the breast cancer marker Her2 on the surface of both fixed and living cancer cells. They also demonstrated the use of luminescent QDs in targeting cellular organells. Their results showed that under the same irradiation conditions, QDs exhibited higher photostability than organic dyes.

Another active research area involving QDs is their application in quantitative bioanalysis. In protein and DNA chips, organic dyes have been widely used for drug screening and disease diagnostics. However, poor photostability and overlaps between emission peaks have been a problem. To overcome this shortcoming of organic dyes, QDs have been explored as alternative to organic fluorophores in immunoassays and DNA analysis. For example, Goldman et al. (82-83) prepared QDs-antibody conjugates and used them in fluoroimmunoassays for the detection of protein toxin and TNT with detection limits of 10 ng/ml for the toxin and 2 ng/ml for TNT. In another example, Han et al. (84) encapsulated CdSe-ZnS QDs into 1.2 μm porous polystyrene microbeads with different ratios of QDs of different emission colors and formed barcodes for DNA hybridization assays. They prepared QDs of six different emission colors and doped them into polymer beads with 10 different ratios of emission intensity. The QDs doped polymer beads could be used to analyze one million DNA samples in a single detection assay.

CHAPTER TWO: SYNTHESIS AND CHARACTERIZATION OF QUANTUM DOTS

This chapter describes the synthesis procedures for the preparation of luminescent semiconductor QDs in both aqueous solution and organic media. Synthesis procedures involve using aqueous solution, reverse micelles, and the surfactant trioctylphosphine oxide (TOPO) media are described. The advantages and disadvantages of these methods are discussed.

2.1 Synthesis of Ligands Capped CdS QDs

The synthesis procedure was adapted from a method developed by Weller et al. (29). A 0.2 mmol of $Cd(NO_3)_2$ and 0.2 mmol of ligands were dissolved in 200 mL of deionized water and purged with pure nitrogen gas for at least 60 min under magnetic stirring. The ligands include sodium polyphosphate, thioglycerol and cysteine. A 0.2-mmol portion of Na_2S dissolved in 10 mL water was added to the solution using a syringe pump at a flow rate of 0.5 mL/minute. The ligands-capped CdS QDs solution was refluxed while boiling for 10 h under N_2 atmosphere. The solution was then condensed by solvent evaporation to 20 mL. Ethanol was used to precipitate the CdS QDs. The capped CdS QDs precipitate was treated with three repeated cycles of precipitation by ethanol, washing, and redispersion to remove contaminants. The luminescent L-cysteine-capped CdS QDs were then resuspended in a 100-mL 0.05 M Tris-HCl buffer solution at pH 7.2. The concentration of particles was estimated to be 150 μM. Aliquot solutions were used for ion response measurements.

2.2 Synthesis of CdSe-CdS Core-Shell QDs in Aqueous Solution.

The synthesis procedure was modified from a method reported by Tian et al. (85). The formation of CdSe core and CdS shell was conducted at room temperature under nitrogen flow. The growth of CdS capped CdSe was performed at 100°C through prolonged reflux under nitrogen atmosphere. A typical proctol for the synthesis of CdS capped CdSe QDs is described below: 12.3mg $Cd(NO_3)_2$ and 24mg sodium polyphosphate were dissolved in 200ml deionized water in a 250ml three-neck flask equipped with septum. The pH was adjusted to 9.5 by 1M NaOH. After bubbling the solution with high purity nitrogen for 30 min, 100 μl freshly prepared 0.058M NaHSe solution was added to the solution drop by drop through syringe under vigorous stirring. After 20 min, 8.2 mg Na_2S in 10 ml deionized water was injected into the CdSe colloid solution slowly. The molar ratio of S to Se was 5.8. The colloid solution was reflux overnight at 373K.

2.3 Preparation of CdS QDs in Reverse Micelles

The synthesis was modified from a method developed by Lianos et al. (39). Two reverse micelles solutions containing Cd ion and sulfide ions were prepared. Cd^{2+} containing micelles were prepared by mixing 0.2ml of 0.1M $Cd(NO_3)_2$ with 20 ml heptane solution containing 0.1 M bis(2-ethylhexyl) sulfosuccinate sodium salt (AOT). S^{2-} containing micelles were prepared by mixing 0.2 ml of 0.1 M Na_2S with 20ml of heptane solution containing 0.1 M AOT. The mixtures were sonicated until forming transparent homogenous inverse micelles solutions. The water to oil ratio (W/O) in the Cd^{2+} and S^{2-} containing micellar solutions was about 5.5. Light green-yellow CdS QDs were formed immediately after mixing the two micellar solutions. To aggregate the QDs, a dithiol molecule that was used as cross-linking agent was added to the

reverse micelles solution to initiate the formation of quantum dots clusters. In 5 ml CdS QDs reverse micelles solution, 100 microliter 1,6-hexanedithiol was added dropwisely under vigorous magnetic stirring. A yellowish precipitate was formed immediately after the addition of dithiol. The yellowish clusters were collected by centrifugation at 2500 rpm for 10 minutes and washed with heptane three times to remove remnant surfactant and dithiol molecules.

2.4 Synthesis of Water Soluble CdSe-ZnS QDs

2.4.1 Synthesis CdSe core in TOPO/TOP media

The synthesis of CdSe was based a greener route reported by peng et al. (49).The experiment was conducted under inert atmosphere. In a 100 ml one neck flask, 12 mg CdO was dissolved in 150mg lauric acid at 150˚ C, the mixture was then cooled down to room temperature. After adding 3g trioctylphosphine oxide, the mixture was heated to 300˚C, 80mg Se dissolved in 2ml trioctylphosphine was injected into the flask under magnetic stirring. The color of the solution changed immediately after the addition of Se. The solution was kept at this temperature for 3 minutes. Then the heating mantle was removed and the solution was cooled to 30˚C. Anhydrous methanol was added to the 100 ml flask to precipitate the CdSe QDs. The QDs were collected by centrifugation at 3000 rpm for 5 minutes. The precipitated CdSe QDs were washed 3 times with anhydrous methanol to remove unbound surfactant.

2.4.2 Synthesis of CdSe-ZnS core-shell QDs.

The synthesis of ZnS shell was based a method developed by Hines et al. (67). The ZnS shell was grown on the surface of the CdSe core to improve the emission quantum yield. The synthesis procedure is described below: 30mg CdSe QDs were mixed with 3g TOPO in a 50ml

flask. The temperature was raised to 240ºC. Then 60µl $(TMS)_2S$ and 400µl $(Et)_2$ Zn were injected into CdSe QDs solution. The temperature was set at 140ºC and kept constant for 3 hours. Then cooled to room temperature. The CdSe-ZnS QDs were precipitated by anhydrous methanol and collected by centrifugation at 3000 rpm for 5 minutes. The product was washed three times with methanol to remove unreacted chemicals and surfactant.

2.4.3 Synthesis of water soluble CdSe-ZnS QDs

Water soluble QDs was prepared based on a method reported by Alldana et al. (72). The QDs synthesized in TOPO media were capped with a surfactant. As a result they were hydrophobic and only dispersible in organic solvent, such as chloroform and hexane. For biological application, the QDs need to be water-soluble. A typical procedure for preparation water-soluble QDs are described below. 20 mg CdSe-ZnS QDs and 500µl thioglycerol in 50 ml methanol were placed in a 100 ml one neck flask. The pH of the solution was adjusted to about 10. Then the solution was refluxed at 70ºC overnight. The solution was condensed to about 20 ml following addition of ethyl ether to precipitate thioglycerol capped QDs. The QDs were collected by centrifugation at 3000 rpm for 5 minutes and washed three times with ether to remove free thioglycerol. The QDs were then dispersed in 5 ml deionized water for use.

2.5 Characterization of Quantum Dots

2.5.1 Absorption Spectra- Absorption spectra of free QDs in solution and their nanoassemblies were obtained using a Varian UV-VIS-NIR spectrophotometer system, model CARY 500 Scan.

2.5.2 Emission Spectra- Emission spectra of free QDs solution and their nanoassemblies were taken in a quartz cuvette using a PTI Quanta Master luminescence spectrometer equipped with a 75 W xenon short-arc lamp as a light source.

2.5.3 Measurement of Quantum Yield- The quantum yield was measured using PTI Quanta Master luminescence spectrometer by comparing the integrated emission intensity of QDs with that of fluorescein. The absorbances of QDs and fluorescein at their excitation wavelengths were identical and below 0.1 to minimize self absorption. Quantum yield of fluorescein is 95%.

2.5.4 Microscopy-Luminescence images of QDs aggregates and QDs nanoassemblies were obtained using a digital luminescence imaging microscopy system. The system consists of an inverted fluorescence microscope (Olympus IX70) equipped with a 100 W mercury lamp as a light source. The fluorescence images were collected using a 40× microscope objective with NA = 0.9. A filter cube containing a 330-385-nm band-pass excitation filter, a 400-nm dichroic mirror, and a 420-nm long-pass emission filter was used to ensure spectral imaging purity. A high-performance ICCD camera (Princeton Instruments, model BH2RFLT3) was employed for digital imaging of the CdS QDs. A PC microcomputer was employed for data acquisition. The Roper Scientific software WinView/32 was used for image analysis.

2.5.5 Transmission Electron Microscopy- The size and morphology of free QDs and their nanoassemblies were characterized using a JEOL 2010 electron microscope.

2.5.6 X-ray diffraction measurement- The XRD pattern of QDs was obtained using a Philips X’pert diffractometer using Cu Kα=154.056pm as radiation source.

CHAPTER THREE: RESULTS

3.1 Synthesis of QDs

3.1.1 CdSe-CdS QDs

Emission of CdSe-CdS QDs- The QDs synthesized at room temperature showed very broad and weak emission as shown in figure 3.1a. After a prolonged reflux, the photoluminescent efficiency of the CdS capped CdSe QDs was significantly increased with

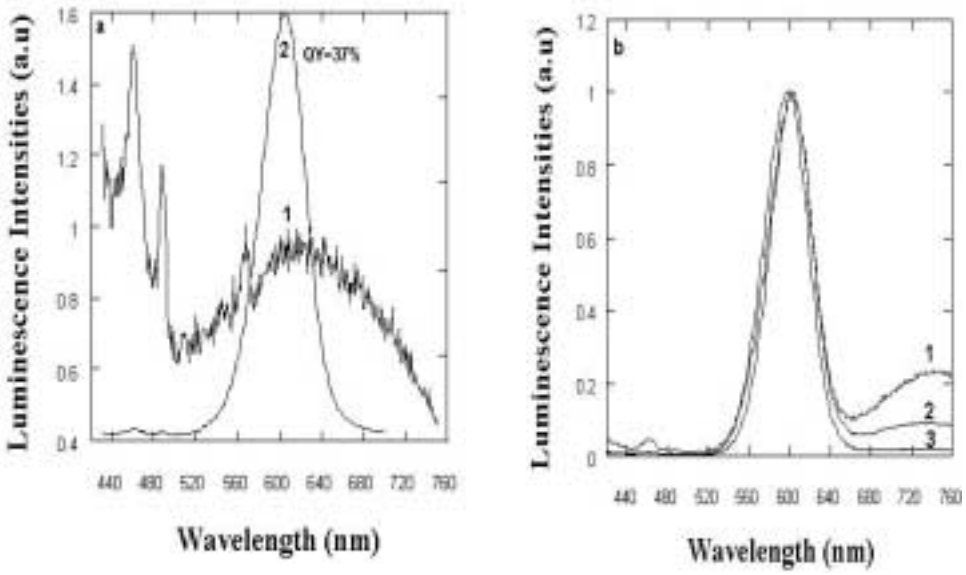

Fig.3.1 (a) Emission spectra of CdS coated CdSe QDs. (1) before reflux; (2) after reflux under atmosphere for 7 hrs. λem=601nm. The quantum yield was about 37%. (b) Shows reflux time has little influence on the emission band of the QDs. (1) 3.5 hrs. (2) 6 hrs. (3) 10 hrs. (c) The strong band-gap emission of CdS capped CdSe QDs shows the surface defects have been removed through prolonged reflux.

quantum yield as high as 37% compared to fluorescein. Without any size-selective precipitation process, the emission spectra of the QDs were very sharp with full width at half maximum (fwhm) less than 45nm. Reflux was critical in this synthesis procedure in order to obtain highly luminescent QDs. Figure 3.1a shows the great difference of the emission intensity before and after reflux. Before reflux, the emission spectrum of CdSe-CdS solution was very broad and weak, however the emission spectrum became very sharp and the emission increased after 12 hours reflux at 100°C. Reflux time has little effect on the emission band of CdS capped CdSe QDs; Figure 3.1b demonstrates the emission band red-shift a few nanometers after reflux. The red tails showed in figure 3.1b curve 1 and 2 were caused by surface defects (86) The surface defects are often attributed to the dangling bonds that can form an additional energy level besides the band gap energy level of the QDs. This additional energy level complicates the relationship between the size of QDs and their emission band position. To overcome this problem a shell with a high band gap energy, such as CdS or ZnS, is usually coated on the surface of CdSe QDs to form a core shell structure. This shell can diminish the surface defects and thus eliminate the red tail. In this case, the red tail was completely removed due to the formation of CdS shell after 10 hours reflux.

Transmission electron microscope image- The size and morphology of the CdS capped CdSe QDs were characterized by JEOL 2010 transmission electron microscope (TEM). The synthesized CdSe-CdS QDs were mostly spherical in shape and had a diameter ranging from 3 to 6 nm depending on the synthetic condition. Figure 3.2 shows a representative TEM image of 4 nm CdSe-CdS QDs. An enlarged TEM image of one single QDs was inserted in figure 3.2. It shows clearly the lattice structure of the CdS capped CdSe nanoparticles. However the CdS shell

can’t be clearly seen because the contrast between CdS and CdSe is low due to the similar electron densities of CdS and CdSe.

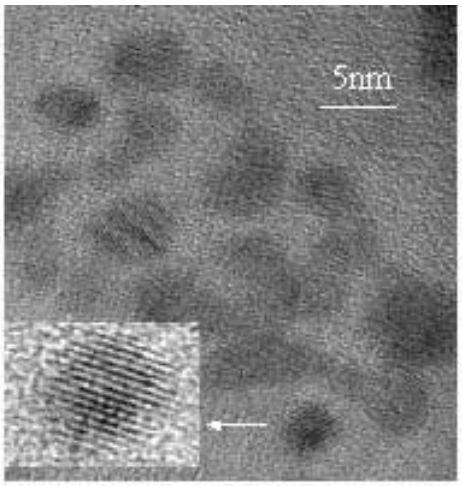

Fig. 3.2 TEM of the CdSe-CdS QDs taken on a JEOL 2010 . Inset is HR-TEM of a selected single QDs, the lattice planes are clearly discernable

X-ray diffraction of CdSe-CdS QDs- A powder X-ray diffraction pattern of CdSe-CdS QDs is shown in figure 3.3. The CdS capped CdSe nanoparticles have well developed crystallinity. The diffraction peaks are broad compared to that of bulk CdSe semiconductor. This is a characteristic of X-ray diffraction pattern of nanocrystals. The 2θ of the XRD peaks are at 26, 43 and 51 degrees. These were assigned to the (111), (220) and (311) lattice planes of the Wurzite, hexagonal structure of the CdSe core. The slight shift of the diffraction peaks to higher angle is attributed to the CdS-CdSe core shell structure (71,87). Although CdS and CdSe share the same Wurzite structure, the XRD peaks of CdS QDs were located at larger angles. The CdS

shell induced a shift of the XRD peaks of the CdSe-CdS core shell nanocrystals to higher angles. Other facts such as various defects in the nanocrystals also affect the diffraction line shape and position. The diameter of the CdS capped CdSe QDs was calculated based on the (111) peak using the Debye-Scherrer formula:

$$d=4L/3,\ L= 0.9\lambda/(\beta\cos 2\theta)\ldots\ldots\ldots(1)$$

where λ is the wavelength of scanning radiation, β is the full width at half-maximum (FWHM) of the (111) peak, and θ is the angle at which the peak is centered. The diameter of QDs was found to be 4.1nm, which was in agreement with the estimated diameter based on TEM measurements.

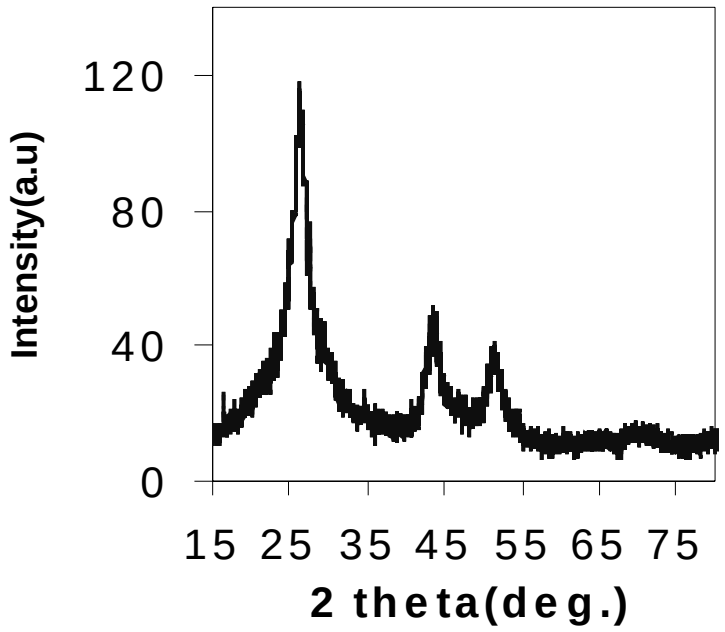

Fig. 3. 3 A powder X-ray diffraction pattern of CdS coated CdSe QDs taken on Philips X'pert diffractometer using Cu Kα=154.056pm radiation.

Synthesis of QDs of different emission colors- By changing the concentration of CdSe cores, the emission band of CdS capped CdSe QDs was tunable from 560nm to 625nm. Generally, the lower CdSe core concentration leads to shorter emission wavelength due to the formation of smaller QDs. Figure 3. 4 shows the series of emission of CdS capped CdSe QDs synthesized through this procedure.

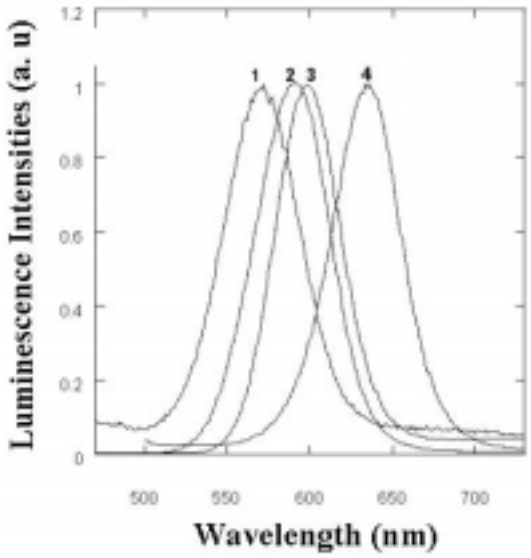

Fig. 3. 4 A series of photoluminescent emission spectra of CdS capped CdSe QDs. (1) λem=560nm; (2) λem=589nm; (3) λem=604nm; (4) λem=625nm

Summary- A simple method without using highly toxic, air-sensitive and expensive organometallic chemicals to synthesize highly luminescent monodispersed CdS capped CdSe QDs in aqueous solution was developed. The quantum yield of CdS capped CdSe QDs was as high as 37%. The emission spectra of ‘as prepared’ CdS capped CdSe were very sharp with

fwhm <45nm without the need of any size-selective precipitation. The emission bands were tunable from 560nm to 625 nm for CdS capped CdSe QDs .

3.1.2. CdS QDs synthesized in reverse micelles

Optical properties- The optical properties of the CdS QDs were characterized by UV-VIS absorption spectrometry using a Varian UV-VIS-NIR spectrometer and by fluorescence spectroscopy using a PTI fluorescence spectrometer. The absorption and emission spectra of a solution containing CdS QDs is shown in the figure 3.5. The broad absorption spectrum enabled the excitation of the CdS QDs at wavelengths ranging from 300 nm to 450 nm. The broad

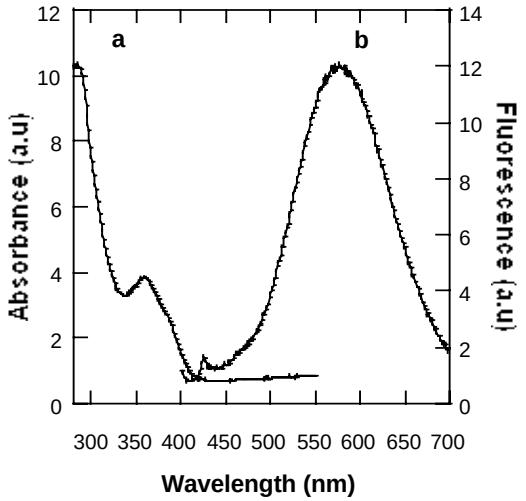

Fig. 3.5 Uv-VIS absorption (curve a) and emission spectra (curve b) of 'as-prepared' CdS QDs in AOT reverse micelles solution.

excitation spectrum provides the flexibility in choosing a suitable wavelength to excite the QDs and minimized the interference from the background emission. A 400 nm light was used for excitation. An emission maximum was observed at 600nm. The red shift of the emission spectrum from the band-edge emission was typical for CdS QDs synthesized at low temperature. The emission of CdS QDs was originated mainly from the surface trapped energy states.

Dithiol initiated aggregation of CdS QDs- 1,6-hexanedithiol contains two thiol groups, one on each end of the carbon chain. Thiol groups have high affinity towards surface cadmium ions. Thus, the dithiol molecules act as cross-linking agents that bridge CdS QDs together to form three-dimensional composites containing CdS QDs. These composites are highly luminescent since many CdS QDs are covalently linked in a single cluster. Figure 3.6 shows the fluorescence images of such CdS QDs aggregates. These luminescent composite materials may find application in light emitting devices.

Fig. 3.6. Fluorescence Images of dithiol Initiated CdS QDs Clusters

Summary- Reverse micelles are effective nanoscale reactors for the synthesis of semiconductor nanoparticles. CdS QDs were successfully synthesized in reverse micelles. However the QDs synthesized in this system usually showed low crystalline quality and low emission efficiency. Surface defects on the QDs form intra band gap energy levels that red shift the emission of the CdS QDs from the band-edge emission. The surface defects also increase the rate of non-radiative relaxation of the excited electrons. The non-radiative relaxation decreases the emission efficiency (88-89). CdS QDs in reverse micelles could be precipitated by dithiols as previously mentioned.

3.1.3 Synthesis of luminescent CdSe-ZnS QDs through CdO-TOPO route

CdSe QDs synthesized in TOPO media showed strong band-edge emission. The emission spectra were sharp with a FWHM about 30nm. Figure 3.7 shows the band-edge emission of CdSe QDs.

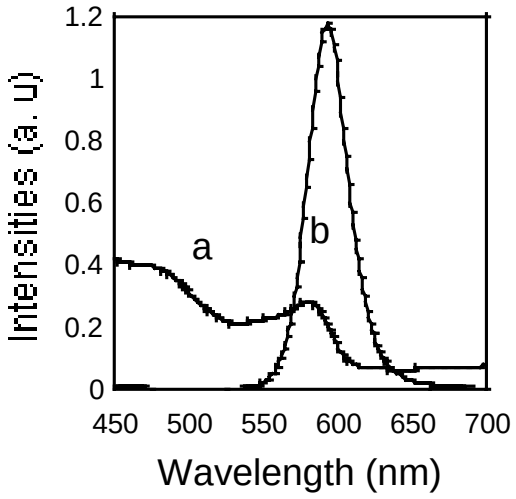

Fig.3.7 Band edge emission of CdSe QDs. (a) absorption spectrum of CdSe QDs. (b) emission spectrum of CdSe QDs.

After coating a ZnS shell on the surface of CdSe QDs, the emission peak usually red-shift 10-20 nm due to the growth of the CdSe QDs core. The emission color of the QDs was tunable by controlling the experimental conditions. Generally, high temperature and long heating time facilitated the preparation of large CdSe QDs. We synthesized a series of QDs of different emission colors including green, yellow and red. The emission spectra are shown in figure 3.8 (A). Figure 3.8 (B) shows photographs of CdSe QDs of different size. The upper row is the image of the QDs when irradiated with room light. The lower photograph shows the emission colors of the QDs when irradiated with UV light. The CdSe-ZnS QDs were brightly luminescent, which is important in biological labeling applications.

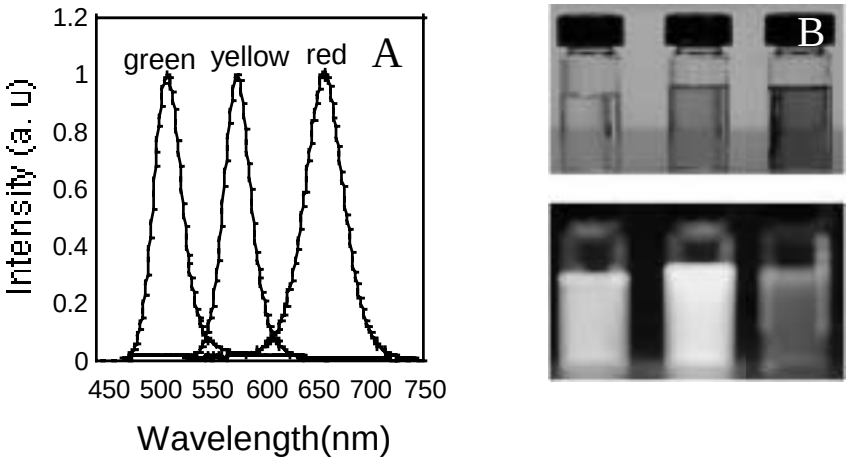

Fig.3.8 (A) a Series of emission spectra of CdSe QDs synthesized through CdO-TOPO route. (B) Images of CdSe QDs at room light (upper row) and under UV lamp irradiation (lower row)

Transmission electron microscope image- QDs synthesized in TOPO media showed high crystallinity. Figure 3.9 shows TEM images of green and red emission QDs. The green emission QDs are about 3 nm and the red emission QDs are about 6 nm in diameter.

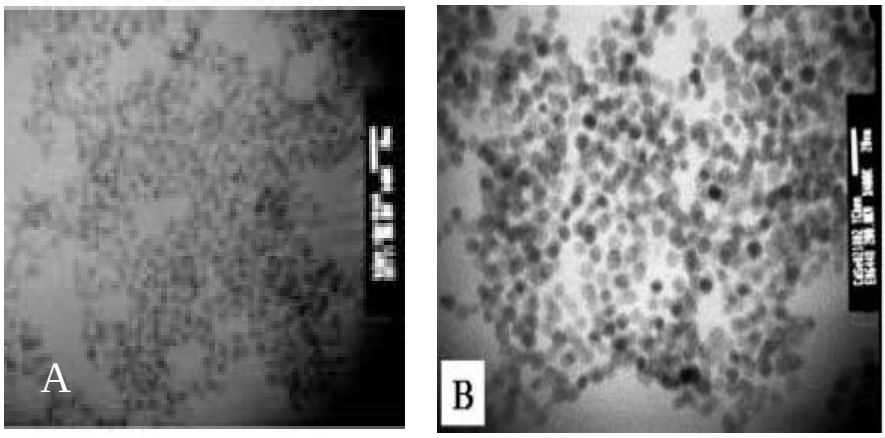

Fig. 3.9. TEM images of CdSe QDs synthesized in TOPO media. (A) green emission QDs , the scale bar is 10 nm. (B) red emission QDs, the scale bar is 20 nm.

Summary- CdSe QDs synthesized in TOPO media were highly crystalline and their emission was size-dependent. By controlling the experimental conditions, green, yellow and red emission QDs were synthesized. The quantum yield was as high as 70% for green emission QDs and 50% for red emission QDs compared to Rhodamine 6G. By capping the CdSe core with a layer of high energy band gap ZnS shell, the stability of CdSe QDs towards the environment was improved. The QDs kept their strong emission after stored at room temperature for more than one year. The CdSe and CdSe-ZnS QDs synthesized in TOP/TOPO media were capped by the surfactant TOPO. Therefore they were only soluble in organic solvents like hexane and chloroform. To apply these high quality QDs in biological systems, they must be transferred

from organic media to aqueous solution. Several methods to prepare water miscible QDs were reported. One method was based on coating the QDs surface with a thin silica layer. The silica layer provided the water compatibility of the QDs and also offered binding sites for further functionalization (90). This method was used to prepare highly stabe water soluble QDs. Another method was based on binding ligands containing thiol groups, such as mercaptoacetic acid or thioglycerol, onto the surface of CdSe-ZnS QDs in chloroform. An aqueous phosphate buffer saline (PBS) solution(pH 7.4) was added to this reaction mixture to extract the ligand capped QDs (72). This method was simpler than the first procedure, however the stability of water soluble QDs was poor. The QDs precipitated in one week due to hydrolysis or oxidation of the capping ligand. Peng et al. (49) developed a method to transfer the QDs to aqueous solution by refluxing the QDs with 11-Mercaptoundecanoic acid in methanol solution. The water soluble QDs prepared through this method were stable for months without significant aggregation(91). In our laboratory, the QDs were transferred to aqueous solution by capping the surface of QDs with thioglycerol. After transferring to aqueous solution, the QDs were still highly luminescent. Other thiol group containing molecules, such as mercaptoacetic acid and mercaptosuccinic acid could also be grafted on the surface of the QDs based on the same procedure. The surface bound carboxylic groups could be used for subsequent conjugation of biomolecules to the QDs.

3.2 Luminescent Semiconductor CdS QDs as Selective Ion Probes

3.2.1 Introduction. Semiconductor QDs have generated great research interest in the past two decades. Many studies in this area focus on the development of new techniques to synthesize high-quality QDs with high-luminescence quantum yield and to measure their photophysical

properties in organic and aqueous media (92-96) . The effect of ionic species on the luminescence of QDs was also studied. For example, Henglein et al. (66) showed that cadmium ions increase the luminescence quantum yield of CdS nanoparticles by about 50% in basic solution. This effect was attributed to the formation of a $Cd(OH)_2$ shell on the CdS core, which effectively eliminates the nonradiation recombination of charge carriers. A similar activation effect was also observed when zinc and manganese ions were added to basic CdS or ZnS colloid solutions(97-98). Weller et al. (99) showed that the emission quantum yield of CdTe nanocrystals stabilized by thioglycolic acid increases with decreasing pH levels. Another study by Kotov et al. (100) showed that binding MoS^{4-} to the surface of CdS nanoparticles induces a red-shift of their excitonic absorption and emission bands as a result of electronic interaction between the anions and CdS nanoparticles. Besides the activation effect mentioned above, some species quench the luminescence of semiconductor nanoparticles. I^- (101) dications of methyl viologen (MV^{2+}), tungsten phosphoric heteropolyacid (PW_{12}) (102), and some of neutral organic molecules, such as butylamine (103-104), and benzyl alcohol (105) effectively quench the emission of CdS or CdSe QDs. Copper ions quench the emission of CdS QDs by forming either Cu_xS (x = 1,2) precipitate on the surface of CdS QDs or isolated Cu^+ on CdS QDs, as proposed by Isarov et al. (106-107). These studies reveal that the luminescence of QDs is sensitive to their surface states. For particles only 1 nm or less in diameter, nearly 100% of the atoms are surface atoms, and no core atoms exist. Thus, it is reasonable to expect that ionic interactions with the surface of luminescent QDs would change their photophysical properties (108).

In the current study, we were able to alter the selectivity of luminescent QDs to certain ions by changing the capping layer of the QDs. The selectivity of luminescent CdS QDs was switched between zinc and copper ions, depending on their capping layer. Although various

fluorescence sensors for copper ions based on organic dyes were previously developed (109-114), these sensors respond to some degree to other divalent cations, particularly zinc ions. This chapter discusses the analytical properties of the luminescent-QDs-based probes and points to future directions in their further development and application in ion analysis in volume-limited biological samples and single cells. The effect of pH, concentration of oxygen and temperature on the emission of thioglycerol capped CdS QDs are also investigated.

3.2.2 Specific experimental details

Materials and reagents. L-Cysteine, cadmium acetate hydrate, cadmium nitrate tetrahydrate, sodium polyphosphate, sodium sulfide nonanhydrate, 1-thioglycerol, *N*,*N*-dimethyl formamide, copper nitrate, zinc sulfate heptahydrate, iron (III) nitrate nonahydrate, sodium chloride, potassium chloride, calcium chloride dihydrate, magnesium sulfate, magnesium chloride hexahydrate, manganese (II) chloride tetrahydrate, and cobalt (II) nitrate hexahydrate were purchased from Aldrich and used as received without further purification. Phen Green FL, *N*-(6-methoxy-8-quinolyl)-*p*-toluenesulfonamide (TSQ) were obtained from Molecular Probes.

Synthesis of polyphosphate capped CdS QDs- Polyphosphate-capped CdS QDs were synthesized as follows: 0.2 mmol of $Cd(NO_3)_2$ and 0.4 mmol of sodium polyphosphate were dissolved in 200 mL of deionized water in a 250-mL three-neck flask. The pH was adjusted to 9.0 with a 1.0 M NaOH solution. A 0.2-mmol portion of Na_2S dissolved in 10 mL water was added into the Cd^{2+} solution through a syringe pump at a flow rate of 0.5 mL/min. The reaction mixture was refluxed while boiling under nitrogen atmosphere for 10 h to obtain bright yellow CdS QDs. The CdS QDs colloid solution was condensed to ~20 mL by solvent evaporation and

then dialyzed against deionized water with a membrane (MWCO 1000) for 4 h. Dialysis was used to purify the polyphosphate-capped CdS QDs rather then precipitation and subsequent washings that are frequently used to purify quantum dots due to difficulties in redispersing precipitated polyphosphate-capped CdS QDs in aqueous solution following precipitation. The dialyzed CdS QDs were diluted in a 100-mL 0.05 M Tris-HCl buffer solution at pH 7.2. The concentration of particles was calculated on the basis of an estimated molar absorption coefficient of 2×10^4 M^{-1} cm^{-1}(29). The final concentration of polyphosphate-capped CdS QDs was ~150×10^{-6} M. This solution was used as a stock solution. Aliquot solutions were used for ion response measurements.

Synthesis of L-cysteine capped CdS QDs- A 0.2 mmol portion of $Cd(NO_3)_2$ and 0.2 mmol of L-cysteine (0.2 mmol) were dissolved in 200 mL of deionized water and purged with pure nitrogen gas for at least 60 min under magnetic stirring. A 0.2-mmol portion of Na_2S dissolved in 10 mL water was added to the solution using a syringe pump at a flow rate of 0.5 mL/minute. The L-cysteine-capped CdS QDs solution was refluxed while boiling for 10 h under N_2 atmosphere. The solution was then condensed by solvent evaporation to 20 mL. Ethanol was used to precipitate the CdS QDs. The cysteine-capped CdS QDs precipitate was treated with three repeated cycles of precipitation by ethanol, washing, and redispersion to remove contaminants. The luminescent L-cysteine-capped CdS QDs were then resuspended in a 100-mL 0.05 M Tris-HCl buffer solution at pH 7.2. The concentration of particles was estimated to be 150 μM. Aliquot solutions were used for ion response measurements.

Synthesis of thioglycerol capped CdS QDs- Thioglycerol-capped CdS QDs were synthesized following a method suggested by Vossmeyer et al. (29) with slight modifications. A 0.2-mmol portion of cadmium acetate hydrate and 0.5 mmol of 1-thioglycerol were dissolved in

50 mL of *N*,*N*-dimethylformamide in a 100-mL three-neck flask. After stirring the solution under N_2 atmosphere for 60 min, 0.3 mmol of sodium sulfide dissolved in 8 mL of deionized water was added to the flask using a syringe pump at a flow rate of 0.5 mL/min. Subsequently, the solution was heated to boiling and kept under reflux for 10 h under N_2 atmosphere. The refluxed solution was condensed to ~20 mL, and absolute ethanol was added to precipitate the thioglycerol-capped CdS QDs. The thioglycerol-capped CdS QDs precipitate was treated with three repeated cycles of precipitation by ethanol, washing, and redispersion to remove contaminants. The luminescent thioglycerol-capped CdS QDs were finally resuspended in 100 mL of 0.05 M Tris-HCl buffer solution at pH 7.2. The concentration of CdS QDs was estimated to be 150 μM. Aliquot solutions were used for ion response measurements.

Photostability measurements- Photostability studies of L-cysteine and thioglycerol-capped CdS QDs and the organic dyes *N*-(6-methoxy-8-quinolyl)-*p*-toluenesulfonamide (TSQ) (zinc ion-sensitive) and Phen Green FL (copper ion-sensitive) were conducted in a Suntest CPS box (Atlas Material Testing Solutions). The irradiation wavelength range was 300-800 nm, and the lamp power was set to 400 W/m^2. Stock solutions (20 mL) of L-cysteine and thioglycerol-capped CdS QDs in a 0.05 M Tris-HCl buffer (pH = 7.2), 20 mL of 2 μM TSQ ethanol solution, and 20 mL of 2 μM Phen Green FL aqueous solution were placed in the chamber for light irradiation. Aliquot solutions were taken periodically for emission intensity measurements.

3.2.3 Results

Synthesis and characterization of CdS QDs- The emission spectra of CdS QDs capped with L-cysteine, thioglycerol, and polyphosphate are shown in Figure 3.10. The emission

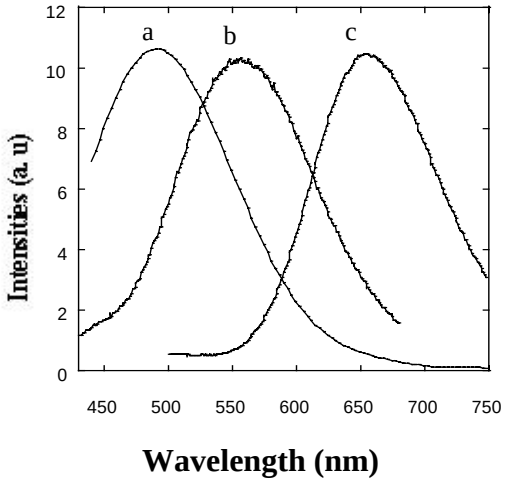

Fig. 3.10 Emission spectra of L-cysteine (a), thioglycerol(b) and polyphosphate(c) capped CdS QDs. The excitation wavelength is 400nm

maxim of L-cysteine, thioglycerol, and polyphosphate-capped CdS QDs are observed at 460, 560, and 650 nm, respectively. The strong red-shift of polyphosphate-capped CdS QDs was previously observed by Lakowicz et al.(101) who discussed the potential of these particles as red luminescent probes in biological samples. Henglein et al. previously established the relation between the absorption threshold of luminescent quantum dots and their diameters (66). Typically, the emission maximum is shifted to longer wavelengths with increasing particle diameter. On the basis of the empirical dependence proposed by Hengelein, the diameter of our L-cysteine, thioglycerol, and polyphosphate-capped CdS QDs are 3, 3.5, and 5 nm, respectively. These results are in agreement with previous studies that showed that the final size of the grown luminescent QDs depends largely on the ligand used to define the boundaries of the nanometric volume used for crystal growth (115). Although the emission peak wavelength depends largely

on the diameter of the particles, it is also affected by their surface states. Surface defects often deteriorate the relation between the band-gap emission and the particle size. Particles with a large number of surface defects show broad and weak emissions, and their emission peaks are often red-shifted. To enhance the band-gap emission, a shell with higher band-gap energy is usually used to coat the surface of the luminescent QDs. For example, ZnS capping has been used frequently to enhance the luminescence of CdS and CdSe QDs. When compared to the emission spectra of QDs synthesized in trioctylphosphine oxide (TOPO) at an elevated temperature, QDs synthesized in aqueous solution generally show wider emission peaks. This suggests that the particles contain a larger number of surface defects. It can be seen that the full width at half-maximum (fwhm) of the particles we synthesize in aqueous solution is ~100 nm, which is 3-4 times wider than the emission peaks of luminescent QDs synthesized in TOPO at elevated temperature. Although transmission electron microscopy (TEM) images of our QDs are in general agreement with the diameter estimated from the emission spectra, the images (not shown) show a variation of up to 50% in the diameter of the particles. This is very typical of QDs obtained through synthetic routes in aqueous media. It should be mentioned that although sharper emission spectra are important in applications involving a multiple number of emission peaks of QDs, they are not imperative for ion response studies that are based on single emission peaks.

Effect of capping ligands on the luminescence response of CdS QDs to metal cations- The effect of the capping ligands polyphosphate, L-cysteine, and thioglycerol on the response of the CdS QDs to 100μ M levels of zinc and copper ions is shown in Figure 3.2 A (polyphosphate capping), B (L-cysteine capping), and C (thioglycerol capping). Figure 3.2 A shows that the luminescence intensity of polyphosphate-capped CdS QDs decreases by 40 and 25% in solutions

containing 100 μM of copper and zinc ions, as compared to the emission of these QDs in an ion-free solution. Figure 3.11 B shows that the luminescence intensity of L-cysteine-capped QDs increases by 2-fold in a solution containing 100-μM zinc ions. These same QDs show a minimal response to the same level of copper ions in the analyte sample. Figure 3.2 C shows that the luminescence intensity of thioglycerol-capped CdS QDs remains unchanged in a 100 μM zinc ion solution. The luminescence of these QDs is quenched by 30% in a solution containing 100 μM copper ions. To better understand the selectivity of L-cysteine- and thioglycerol-capped CdS QDs toward zinc and copper ions, we compared their corresponding ion response with their response to other biologically relevant ionic species. The response of L-cysteine- and thioglycerol-capped CdS QDs to 1 mM levels of biologically relevant ions is shown in Figure 3.12 A and B, respectively. The

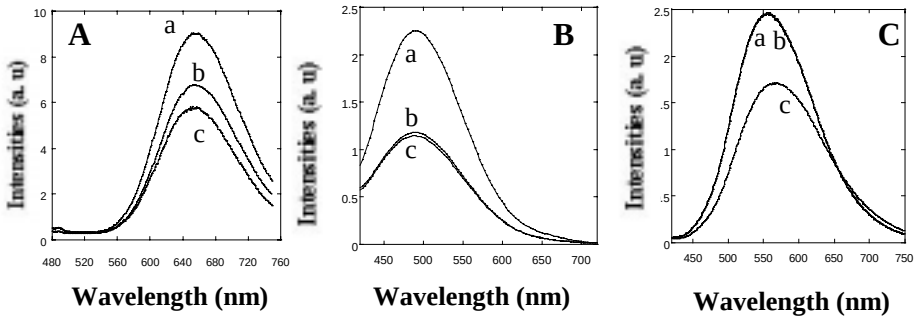

Fig. 3.11. Effects of 100 μM of zinc ions and copper ions on the luminescence of CdS QDs capped with different ligands. (A) Polyphosphate-capped CdS QDs showing no selectivity to copper and zinc ions: (a) ion-free sample; (b) 100 μM zinc ions; and (c) 100 μM copper ions. (B) L-Cysteine-capped CdS QDs showing selective response to zinc ions: (a) 100 μM zinc ions; (b) ion-free sample; and (c) 100 μM copper ions. (C) Thioglycerol-capped CdS QDs showing selective response to copper ions: (a) ion-free sample; (b) 100 μM zinc ions; and (c) 100μ M copper ions.

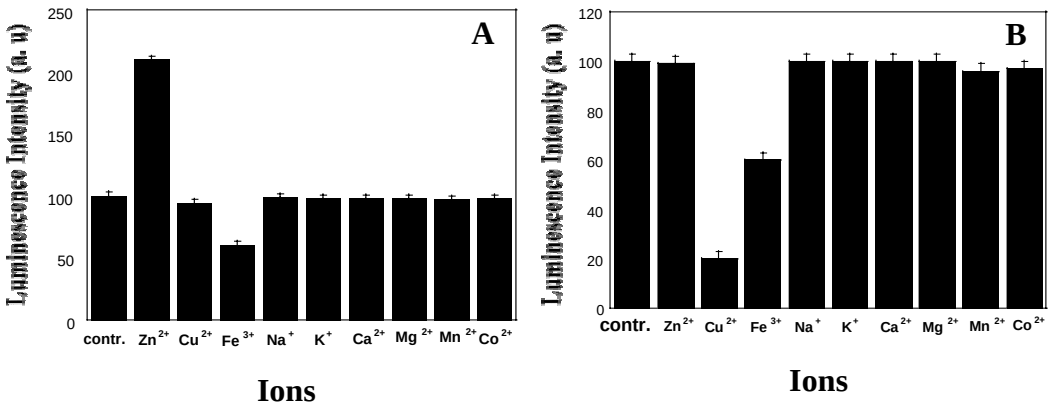

Fig. 3. 12 Effect of 1 mM biologically relevant ions on the luminescence of (A) L-cysteine and (B) thioglycerol-capped CdS QDs.

luminescence intensity of L-cysteine capped CdS QDs is minimally affected by copper, calcium, and magnesium ions. The luminescence of these QDs increases by ~2-fold in a 1 mM zinc ion solution. It should be noted that $Zn(OH)_2$ is not formed when mixing Tris-HCl (pH = 7.2) buffer solution with zinc ions, even at millimolar concentrations. Thus, we believe that the activation of the QDs is not due to the formation of $Zn(OH)_2$ on their surface. The luminescence increase is rather attributed to the formation of a zinc-cysteine complex on the surface of the QDs. A digital luminescence image of a 100 μM L-cysteine-capped CdS QDs in a 100 μM zinc ion solution is shown in Figure 3.13. Aggregates of CdS QDs formed after 10 min of mixing are clearly observed. These aggregates are formed at relatively high zinc ion and QDs concentrations by zinc ions that bridge between L-cysteine-capped CdS QDs to form a three-dimensional CdS QDs network. Other bivalent cations, such as calcium and magnesium ions, do not initiate such aggregate formation. Zinc ions do not induce aggregation of thioglycerol- or polyphosphate-capped CdS QDs. In addition, the aggregation of the L-cysteine-capped CdS QDS does not take

place in a zinc ion-free solution. These observations support our claim that the interaction between zinc ions and the L-cysteine capping of the QDs is the basis for the selectivity of L-cysteine-capped QDs toward zinc ions.

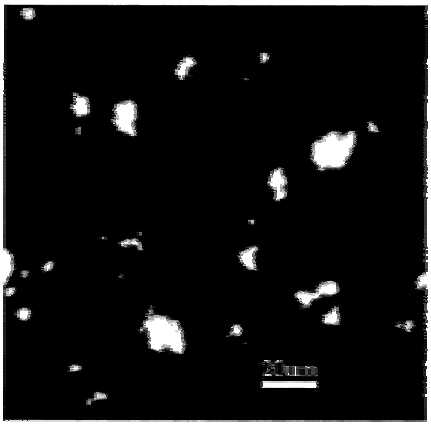

Fig 3.13. Luminescence image of 100 μM L-cysteine-capped CdS QDs clusters mediated by a 15-min exposure of the QDs to a solution containing 100 μM zinc ions. The scale bar is 20 μM.

Figure 3.12 B shows that the luminescence intensity of thioglycerol-capped CdS QDs is insensitive to zinc and other cations at a level of 1 mM. Only copper and iron ions quench the luminescence of these QDs. The effective quenching and red-shift of the luminescence of thioglycerol-capped CdS QDs in response to copper ions is attributed to effective electron transfer from the thioglycerol to the copper ions. The reduction of Cu^{2+} to Cu^{+} by thioglycerol forms CdS^{+}-Cu^{+} species on the surface of the QDs. Isarov et al. (106) demonstrated that CdS^{+}-Cu^{+} has a lower energy level than pure CdS QDs. This new energy state is responsible for the red-shift of the luminescence of CdS QDs from 560 to 610 nm in our experiments. Moreover, Cu^{+} effectively quenches the luminescence of thioglycerol-capped CdS QDs by facilitating

nonradiative recombination of excited electrons (e^-) in the conduction band and holes (h^+) in the valence band. The unique ability of thioglycerol to reduce copper ions may explain the selective response of thioglycerol-capped CdS QDs toward copper ions. The quenching effect of Fe^{3+} on the luminescence of L-cysteine and thioglycerol-capped CdS QDs is attributed to an inner filter resulting from the strong absorption of the excitation wavelength by Fe^{3+}. The transmission of a Tris-HCl pH 7.2 buffer solution containing 1 mM of Fe^{3+} at 400 nm (the excitation wavelength of our QDs) is only ~10%. Forming the colorless complex FeF_6^{3-} by adding fluoride ion to the solution eliminates this inner filter effect. Figure 3.14 Showed in the presence of 1 mM of F- ions, the inner filter effect was effectively eliminated. The emission of thioglycerol capped CdS QDs did not quench by iron ions.

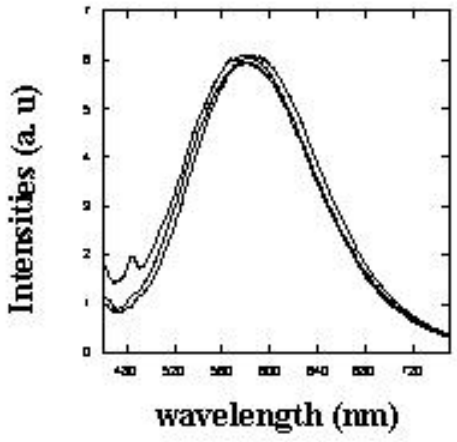

Fig. 3.14 After formation of colorless FeF_6^{3-} complex, Fe^{3+} ions have no inner filter effect to the excitation irradiation. The emission of thioglycerol capped CdS QDs is insensitive to FeF_6^{3-}. [Fe^{3+}] = 0,100μM, 500μM.

Ion analysis properties of L-cysteine and thioglycerol capped CdS QDs- The zinc ion concentration dependence of the luminescence intensity of L-cysteine-capped CdS QDs is shown in Figure 3.15. Curve 3.15 A shows that the emission intensity of L-cysteine-capped CdS QDs increases sharply in response to zinc ions. The dynamic range is up to 20 μM, and the detection limit is ~0.8 μM. The estimated standard deviation for five replicate measurements of a solution containing 10 μM zinc ions is 0.18. Therefore the luminescent intensity of individual measurement at 10 μM of zinc ions was within $I \pm 3\times 0.18$ with 99% confidence level (where I was the average luminescent intensity). The errors were labeled on the figures as error bars. The concentration dependence of the luminescence intensity follows the binding of zinc ions to the surface of the L-cysteine-capped CdS QDs and is effectively described by a Langmuir-type

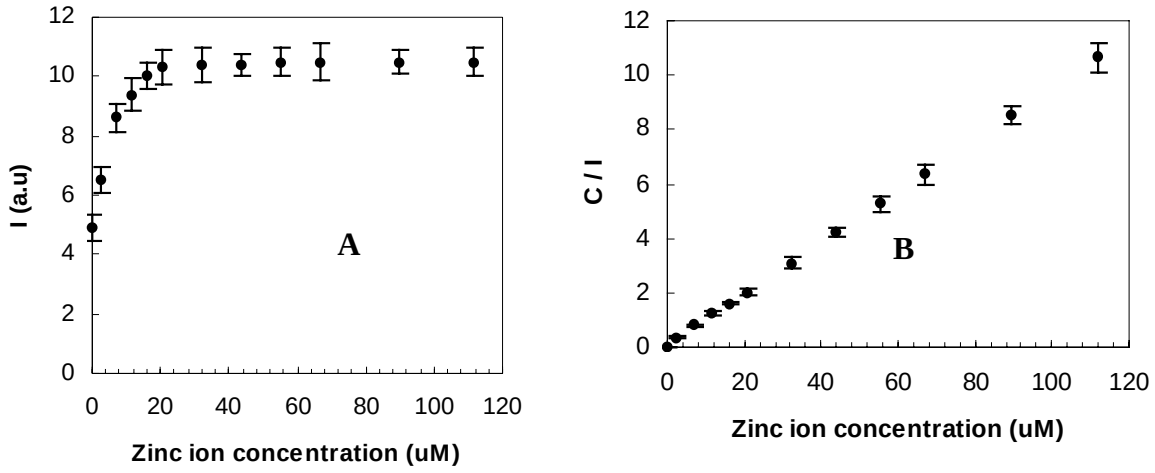

Fig. 3.15 (A). Effects of zinc ion concentration on the luminescence of L-cysteine-capped CdS QDs showing increasing emission with increasing zinc ion concentrations. (B) Langmuir binding isotherm description of the data showing a linear fit throughout the zinc ion concentration range, with a binding constant of 0.89 and a correlation coefficient >0.99.

binding isotherm (116). The luminescence intensity increases with increasing zinc ion concentrations, but then levels off with the decreasing availability of binding sites. According to Langmuir, the surface of the quantum dots consists of a finite number of binding sites. Each of the binding sites could absorb one ion from the solution. The fraction of occupied sites is defined as θ. The rate of binding of ions to the surface is proportional to the ion concentration *C* in the analyte solution and to the fraction of available binding sites 1 -θ. The rate of binding, R_b, of ions to the surface is expressed as

$$R_b = K_b C(1 - \theta) \qquad (1)$$

The rate of desorption of bound ions from the surface depends only on the fraction of occupied binding sites and is expressed as

$$R_d = K_d \ \theta \qquad (2)$$

The rate of binding is equal to the rate of desorption at equilibrium

$$K_d \theta = K_b C (1- \theta) \qquad (3)$$

The equation can be solved for θ as a function of the ratio $B = K_b/K_d$.

$$\theta = (BC) / (1 + BC) \qquad (4)$$

The fraction of occupied binding sites, θ, is related to the ratio between the signal obtained at a given ion concentration *I* and the maximum intensity I_{max}.

$$\theta = I / I_{max} \qquad (5)$$

Therefore an expression that relates the ion concentration, *C*, to the signal intensity can be written as

$$I/I_{max} = (BC)/ (1+ BC) \qquad (6)$$

This equation could be linearized to take the form

$$C/I = (1/BI_{max}) + (1/I_{max})\, C \qquad (7)$$

Accordingly, if the Langmuir description of the binding of zinc ions on the surface of the L-cysteine-capped CdS QDs is correct, a plot of *C*/*I* as a function of *C* should be linear. The dependence of *C*/*I* as function of *C*, where *C* is the zinc ion concentration and *I* is the luminescence intensity of the L-cysteine-capped CdS QDs at given zinc ion concentrations, is shown in Figure 3.6 (B). Based on the principle of propagation of error, the estimated standard deviation of C/I (assuming C was a constant) was:

$$S_{C/I} = C / I^2 * S_I \qquad (8)$$

where $S_{C/I}$ was the standard deviation of C/I; S_I was the standard deviation of the intensity at zinc concentration of C. When zinc concentration C = 20 μM, the standard deviation of C/I was calculated to be 0.035. A very high linearity is observed throughout the entire range of zinc ion concentration. The binding constant *B* is found to be 0.89, and the correlation coefficient of the linear fit is higher than 0.99. The remarkable Langmuirian fit suggests that the probability of binding more than one ion to the surface of an individual QDs, which is imperative for aggregation or a non-Langmuir binding isotherm due to island formation, is negligible under our experimental conditions. It should be mentioned that the luminescence of the cysteine-capped CdS QDs was measured a few seconds after adding the zinc ions to the sample. As previously described, zinc ions induce aggregation of the QDs in a slow process that takes over 10 min and requires high concentrations of zinc ions and L-cysteine-capped CdS QDs to complete. Deviations from the Langmuir behavior could occur as a result of aggregation or islanding of the QDs during ion exposure. The submicromolar zinc ion sensitivity realized in our L-cysteine-capped QDs might not be sufficient for quantitative zinc ion release measurements and intracellular analysis of zinc ions in single cells (117). It is, however, sufficient to follow in real time the kinetics of the release of zinc ions from zinc ion-containing neuronal vesicles. These vesicles contain up to millimolar levels of zinc ions (118).

Figure 3.16 (A) describes the copper ion concentration dependence of the luminescence intensity of thioglycerol-capped CdS QDs. It can be seen that the luminescence intensity decreases with increasing copper ion concentration. Furthermore, a red-shift of ~50 nm is observed with increasing copper ion concentration. As previously mentioned, this red-shift indicates the formation of CuS^+ on the surface of the QDs. The luminescence intensity of the

thioglycerol-capped CdS QDs in a 1.6 mM copper ion solution at 560 nm is 7 times lower than their luminescence intensity in a copper ion-free solution. The estimated standard deviation for five replicate measurements of a solution containing 1 μM copper ions was 0.054. The real value of the measurement was within I ± 3× 0.054 with 99% confidence level (I was the average intensity at 1 μM of copper ion). The response time of the thioglycerol-capped CdS QDs to 25 μM Cu^{2+} was <1 s. An attempt to fit a Langmuir-type binding model to describe the copper ion concentration dependence of the luminescence intensity of the thioglycerol-capped CdS QDs has failed. We found that copper ions quench the luminescence of the QDs in a concentration dependence that is best described by a Stern-Volmer-type equation:

$$I_{max} / I = 1 + K_{sv}[Q] \qquad (9)$$

I and I_{max} are the luminescence intensities of the thioglycerol-capped CdS QDs at a given copper ion concentration and in a copper ion-free solution. *Q* is the copper ion concentration. Figure 3.7 B shows a Stern-Volmer quenching curve describing I_{max}/I as a function of copper ion concentration. K_{sv} is found to be 2800 M^{-1}. Since the estimated standard deviation of five replicate measurement at 1 μM copper ion concentration was 0.048, based on propagation of error, the estimated standard deviation of $Y= I_{max}/I$ could be calculated using the equation:

$$S_y^2 =(S_{max}^2/I^2 + I_{max} * S_I^2 /I^4) \qquad (10)$$

where S_y was estimated standard deviation of I_{max}/I ; S_{max} and S_I were the estimated standard deviation of I_{max} and I.

When copper ion concentration was 500 μM, the estimated standard error of I_{max}/I was calculated to be 0.047. However, conversely to typical Stern-Volmer quenching behavior, which is driven by collisions between quencher and luminescent molecules, the quenching of the luminescence of the QDs is attributed to ion binding followed by a redox reaction on the surface of the QDs. This results in a nonreversible luminescence quenching similar to the one observed when antibodies against fluorescence dyes such as fluorescein, rhodamine, and Texas Red bind to their corresponding antigens (119). Since the response of the CdS QDs to copper ions is not reversible, they cannot be used for real-time monitoring of large ion waves. Nevertheless the large dynamic range enables multiple determinations of copper ion concentrations in diluted copper ion solutions.

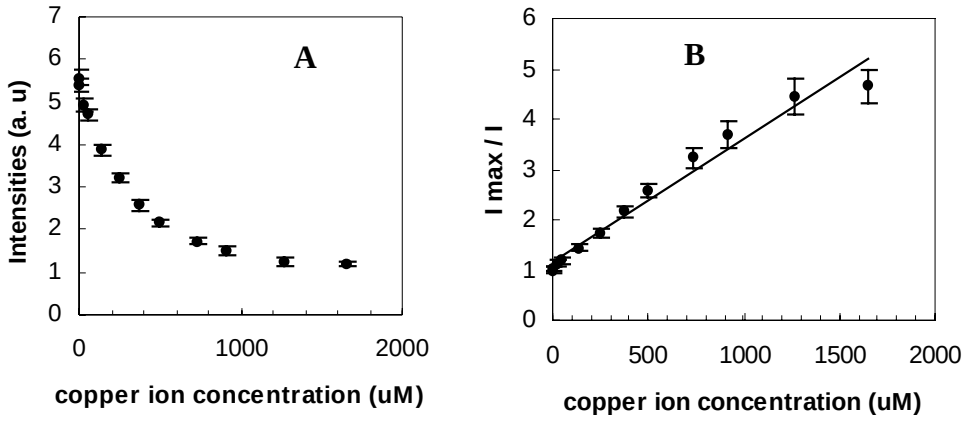

Figure 3.16 (A) Effect of copper ion concentration on the luminescence of thioglycerol-capped CdS QDs showing that copper ions quench the emission of the thioglycerol-capped CdS QDs. (B) A Stern-Volmer plot effectively describes the copper ion concentration dependence of the luminescence intensity of the thioglycerol-capped CdS QDs with a Stern-Volmer constant K_{sv} = 2800 M^{-1}.

Photostability of L-cysteine and thioglycerol capped CdS QDs- Similarly to organic fluorophors, the luminescence of L-cysteine and thioglycerol-capped CdS QDs decreases when continuously irradiated by light with a wavelength from 300 to 800 nm (400 W/cm^2). However, they are still more photostable than organic dyes commonly used for zinc and copper ion fluorescence detection. Figure 3.17 (A) shows a comparison between the photostability of L-cysteine-capped CdS QDs and 2 μM *N*-(6-methoxy-8-quinolyl)-*p*-toluenesulfonamide (TSQ), a commonly used zinc ion indicator. The QDs solution was diluted to obtain an emission intensity similar to that of the 2 μM TSQ solution. The luminescence of the TSQ ethanol solution decreased by about 90% when irradiated for 60 min. Conversely, the emission of L-cysteine-capped CdS QDs decreased by only 30% under similar illumination conditions. Figure 3.8 (B) describes the luminescence intensity of thioglycerol-capped CdS QDs and 2 μM Phen Green FL, a commonly used copper ion

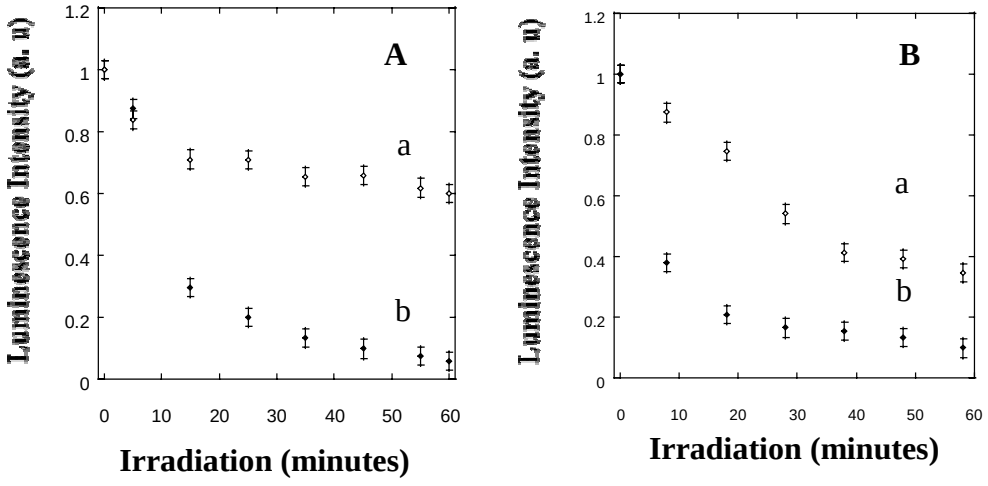

Fig. 3.17 Photodecomposition rate of L-cysteine- and thioglycerol-capped CdS QDs and fluorescence dyes: A) photodecomposition curves of L-cysteine-capped CdS QDs and the zinc-sensitive organic dye TSQ, and (B) photodecomposition curves of thioglycerol-capped CdS QDs and the copper ion-sensitive dye Phen Green FL

fluorescence indicator. Again, the QDs solution was diluted to obtain an emission intensity similar to that of the 2 μM Phen Green FL solution. The luminescence intensity of the thioglycerol-capped CdS QDs decreased by ~20%, whereas the fluorescence intensity of Phen Green FL decreased by nearly 80% following 20 min of irradiation. Peng and co-workers recently attributed the photochemical relative instability of thiol-coated CdSe nanocrystals to photocatalytic oxidation of the thiol ligands on the surface of their surface (72). It is probable that the limited photodecomposition of our thioglycerol-capped CdS QDs was caused by a similar oxidation process.

Effect of pH, O_2 and temperature on thioglycerol capped CdS QDs - The effect of the pH on the emission intensity of thioglycerol capped CdS QDs is shown in figure 3. 18(A). The emission of thioglycerol capped CdS QDs in a solution of pH 7.2 is 34% higher than the luminescence of the same solution at pH 8.0. Molecular oxygen is an effective quencher of the fluorescence of organic dyes. As shown in figure 3.19 (B), it also quenches the emission of thioglycerol capped CdS QDs. The emission intensity of a nitrogen saturated thioglycerol capped CdS QDs solution is 20% higher than the emission intensity of thioglycerol capped CdS QDs in an air-saturated solution and 70% higher than the emission intensity of thioglycerol capped CdS QDs ın a oxygen saturated solution. Similarly to quenching of organic fluorophors by oxygen the quenching of thioglycerol capped CdS QDs is also reversible. The emission intensity is restored to its air saturated level when N_2 or O_2 saturated solutions are exposed to air for about 10 minutes. The luminescence of the thioglycerol capped CdS QDs is also temperature dependent. Figure 3.19 shows that the emission intensity decreases with increasing temperature. Bavykin et al. (105) recently attributed this effect to increasing efficiency of nonradiative deactivation

processes with increasing temperature. To eliminate the effect of pH, O_2 and temperature on the luminescence of thioglycerol capped CdS QDs, our Cu^{2+} measurements were conducted in a Tris-HCl buffer solution at pH 7.2 at room temperature and ambient atmosphere.

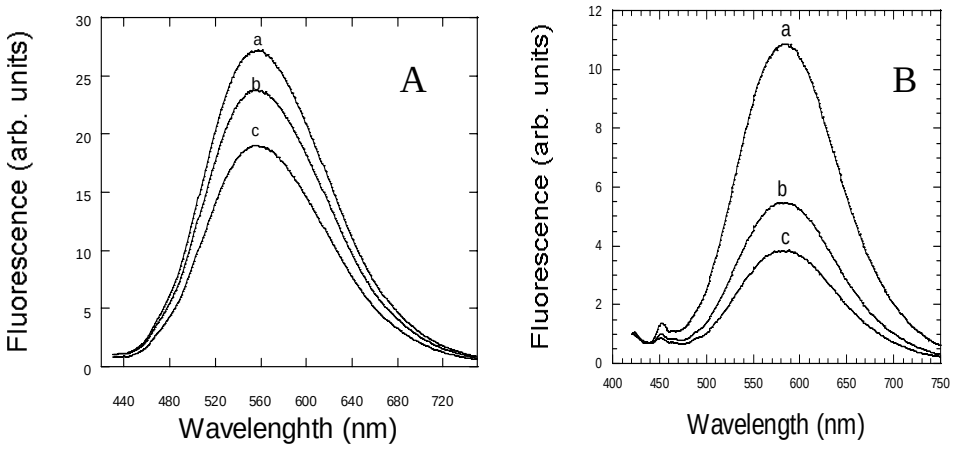

Fig. 3.18. (A) Influence of pH and O_2 on the luminescence of thioglycerol capped CdS QDs. (a) pH=3.0, (b) pH=7.2, (c) pH = 8.0. Influence of O_2 on the luminescence of thioglycerol capped CdS QDs. (B) (a) N_2 saturated (b) air saturated and (c) O_2 saturated. O_2 has a significant quenching effect on the luminescence of thioglycerol capped CdS QDs

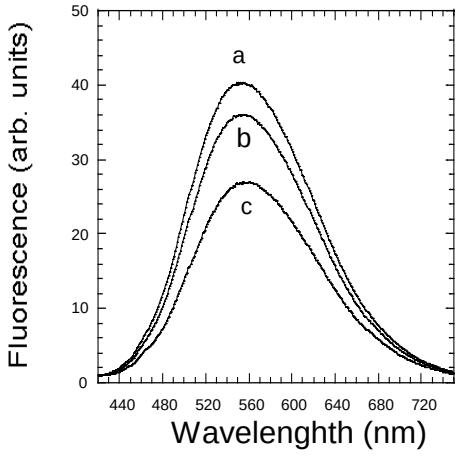

Fig.3.19. Influence of temperature on the luminescence of thioglycerol capped CdS QDs. (a) 277 K, (b) room temperature, (c) 323 K. The luminescence is weak at higher temperature, and the intensity change is reversible

3.2.4 Summary

Luminescent semiconductor QDs have been used as luminescent labels in cellular biology applications. These luminescent nanocrystals are an attractive alternative to fluorescent particles containing organic fluorophors because of their higher photo- and chemical stability in biological systems, narrow spectral bandwidth, and wide range of emission colors. To date, luminescent QDs have been applied in biological systems only as luminescent labels. This paper describes for the first time the quantitative application of luminescent semiconductor QDs in ion analysis. The effect of three different ligands on the luminescence response of CdS QDs to biologically important ions was investigated. L-Cysteine-capped CdS QDs show a selective response to zinc ions and have minimal or no response to other cations. A Langmuir-type binding model is highly effective in describing the zinc ion concentration dependence of the luminescence intensity of the L-cysteine-capped CdS QDs. Thioglycerol-capped CdS QDs show high sensitivity and high selectivity toward copper ions. Other cations do not interfere with copper ion analysis. A Stern-Volmer equation effectively describes the copper ion concentration dependence of the luminescence intensity of the thioglycerol-capped CdS QDs. The insensitivity of the thioglycerol-capped CdS QDs to zinc ions is of particular importance, since zinc and copper ions elucidate an interfering response from fluorescent organic indicators. One should also be aware of inter filter effects that may interfere with zinc or copper ion analysis. For example, iron (III) interferes strongly with zinc and copper ion analysis due to the large absorption coefficient in the excitation wavelength range used in our measurements (~400 nm). Adding F^- ions to the sample to form the colorless complex FeF_6^{3-} eliminates this inner filter effect. The selectivity, sensitivity and limit of the detection of the L-cysteine and thioglycerol-capped CdS QDs enable the measurement of zinc and copper ion concentrations in biological samples. However, several

problems still need to be solved before luminescent QDs can be employed to analyze ion levels in biological samples and single cells. Because of the large number of possible interfering agents, there is a clear need to coat the luminescent QDs with a protective layer that would not only be permeable to the analyte of interest but would also protect the QDs core from interfering substances. The signal-to-noise ratio in microscopy measurements needs to be improved to facilitate ion binding measurements at the individual QD level. The use of laser-based microscopy systems may enable such measurements. Another possibility is to create organized nanometric clusters of QDs to yield larger emission signals. Since QDs tend to aggregate in solutions containing high salt levels, there is also a need to ensure that the capping ligands of the QDs can prevent their aggregation in physiological buffers. Current studies in our laboratory are focused on eliminating interference by blood components that largely absorb light at 400 nm. We are now preparing ligand-capped CdSe QDs with an excitation wavelength of about 480 nm, which is more suitable for blood analysis. We are also developing QDs with increased sensitivity toward zinc ions. In the new QDs, the L-cysteine capping ligand is replaced with a zinc ion binding peptide to increase the binding constant between zinc ions and the CdSe QDs. This may enable the use of the zinc ion-sensitive QDs for real-time zinc ion release measurements in single neuron cells.

3.2 Quantum Dots Nanoassemblies and Their Application as Bioprobes

This section describes three novel methods to encapsulate CdSe QDs in nanospheres including glyconanospheres, micelles and silica nanospheres and their application as bioprobes in immunoassay.

3.3.1 Stabilized luminescent CdS-ZnS QDs encapsulated glyconanospheres

3.3.1.1 Introduction

Incorporation of luminescent semiconductor QDs into nanospheres has been explored as a way to prepare bright biological labels and functional composite luminescent materials. For example, Barbara-Guillem (120) successfully encapsulated luminescent CdSe QDs and other metal oxide nanocrystals in nanometric liposomes for potential biological labeling applications. Rogach et al. (121) encapsulated CdSe QDs in 40-80 nm silica nanospheres and proposed to use them as building blocks to form 3D colloid crystal microstructures. Moffitt et al. (122) encapsulated CdS QDs in water-soluble block copolymers to form large compound micelles (LCM) that averaged 65 nm in diameter. In another study, Han et al. (84) doped 1.2 μm polystyrene microspheres with ZnS-coated CdSe QDs of several emission colors. The particles were used for multiplex optical coding in DNA hybridization assays. The encapsulated QDs showed even narrower emission spectra compared to free QDs. While QD-doped polymer particles of micrometric dimensions have found use in various bioanalytical applications there is still a need for composite nanometric structures of QDs. For example, spheres of nanometric dimensions would be more suitable for cytoplasmic intracellular measurements because nanometric particles could escape endocytosis with higher efficiency. Furthermore, composite materials of nanometric dimensions would provide higher spatial resolution and could be directed to volume-limited samples such as dendrites of neuron cells. Common disadvantages of these structures have been their lack of surface functional groups that are suitable for further bioconjugation and limited chemical stability and biocompatibility. Here, we describe for the first time the development of CdSe-ZnS QD incorporated luminescent glyconanospheres that are suitable for bimolecular conjugation while maintaining the high emission quantum yield of the QDs. The glyconanospheres contain dextran molecules on their surface that interact strongly

with carbohydrate binding proteins (CBP). These novel glyconanospheres could be used for real-time monitoring of protein carbohydrate interactions.

The basis for the preparation of the glyconanospheres is electrostatic interaction. Electrostatic interactions of polyelectrolytes have been widely applied in layer-by-layer procedures to prepare thin films since Decher et al. introduced this unique technique in the early 1990s (123-124). Using this technique, Anai et al. (125) successfully incorporated the highly charged protein avidin into a thin film and used it to immobilize biotinylated molecules. Caruso et al. (126) immobilized enzymes on the surface of polystyrene microspheres to fabricate micrometric biocatalyst carriers using the same layer-by-layer approach. Goldman et al. (83) prepared bioinorganic conjugates by using negatively charged CdSe-ZnS QDs and positively charged avidin. They used these new particles for luminescence immunoassay applications. In their study, the concentrations of QDs and avidin were limited to minimize aggregation due to electrostatic attractions. In the current study we use electrostatic interactions to incorporate negatively charged CdSe-ZnS QDs into luminescent nanospheres that contain polysaccharides on their surface. While DNA and protein molecules were already conjugated to luminescent semiconductor QDs (127-128). we demonstrate for the first time the synthesis of QD-polysaccharide nanocomposites.

3.3.1.2 Specific experimental details.

Materials- mercaptosuccinic acid, trioctylphosphine oxide, trioctylphosphine, dextran, chloroacetic acid, cadmium oxide, lauric acid, diethyl zinc (0.1M solution in heptane),

hexamethyldisilanthiane were purchased from Aldrich and used as received without further purification.

Synthesis water soluble CdSe-ZnS QDs- Water soluble mercaptosuccinic acid capped CdSe-ZnS QDs were synthesized based on the procedure described in chapter two.

Synthesis of carboxymethyldextran (CM-dextran)- Carboxymethyldextran (CM-dextran) was prepared by mixing 100 mg dextran with a molecular weight of 10 000 Da with 200 mg chloroacetic acid in a 6N NaOH alkaline solution at 60 °C for 1 h following a procedure first suggested by Rebizak et al.(129). The CM-dextran solution was neutralized by titrating HCl following dialysis in pure water overnight.

Preparation of the luminescent glyconanospheres- 300 μL aqueous solution of 500 μM CM-dextran was mixed with 120 μL aqueous solution of 0.19 μM mercaptosuccinic acid modified CdSe-ZnS QDs. The concentration of the CdSe-ZnS QDs was calculated using molecular extinction coefficients previously reported by Striolo et al. of 1.1×10^6 M^{-1} cm^{-1} for 3 nm sized CdSe-ZnS QDs and 1.22×10^6 M^{-1} cm^{-1} for 6 nm sized CdSe-ZnS QDs (130). Then, 120 μL of 10 μM polylysine in a pH 7.0 phosphate buffer solution was added to the CM-dextran and QD containing solution. The reaction mixture was incubated at room temperature for 30 min. The newly formed glyconanospheres were washed three times using centrifugation at 4500 rpm for 15 min to remove unreacted QDs and CM-dextran.

3.3.1.3 Results

Choose of the precursors- Three precursors are used to prepare the QDs doped

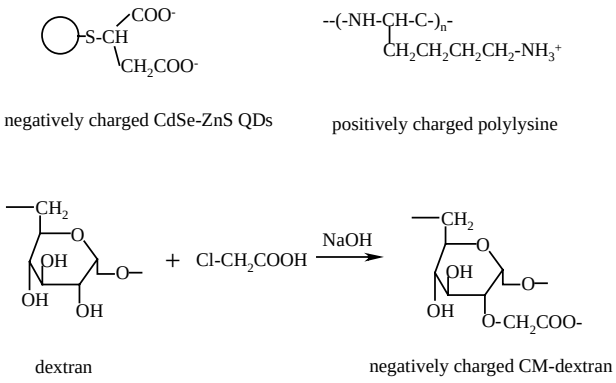

Fig. 3.20 Molecular structures of three precursors

glyconanospheres. Their structures are shown in figure 3.20. The CdSe-ZnS QDs are capped by mercaptosuccinic acid in this study. Each mercaptosuccinic acid molecule contains two carboxylic groups, these groups make the QDs highly water soluble. Carboxylic groups also provide high density negative charge on the surfaces of QDs. Dextran is a highly branched polysaccharide that has no net charge. Each dextran molecule contains many α-D-glucose residues. To incorporate dextran in QDs containing nanospheres, electric charges are needed. In this study, carboxylic groups are grafted onto dextran molecules. The average number of carboxylic group per glucose residue is 0.5 (129). Due to high molecular weight of dextran used in this study (MW=10,000), each dextran molecule contains about 30 carboxylic group (the glucose residues are calculated to be about 60 in each dextran molecule). Therefore the carboxylic groups make the dextran highly negatively charged. Polylysine is well known for its

high density of positive charge. It has been used widely to immobilize cells on glass slide due to its high affinity towards negatively charged glass slide. Polylysine is used to precipitate both QDs and CM-dextran through electrostatic interaction.

TEM imaging of glyconanospheres- Figure 3.21(A) shows a representative TEM image of as-prepared luminescent glyconanospheres. The spherical nanospheres average 190 nm in diameter. Figure 3.21 (B) shows a high-resolution TEM image focusing on a single glyconanosphere. The nanometric CdSe-ZnS QDs are clearly seen as darker dots

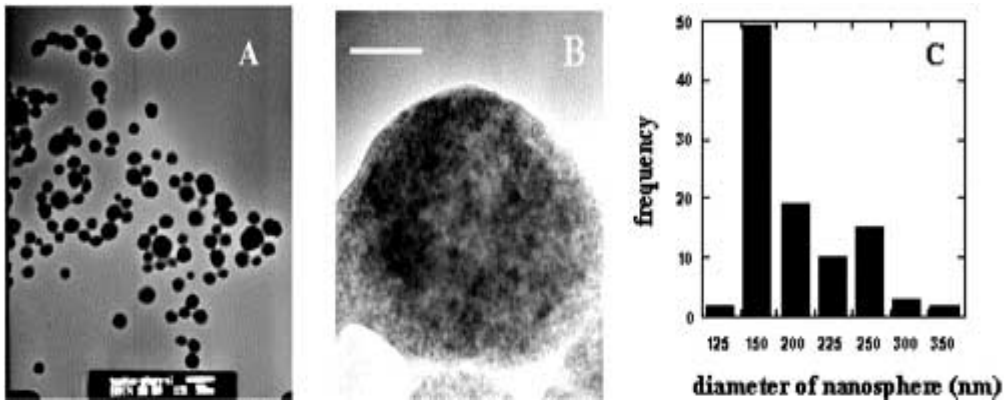

Fig. 3.21 TEM images of as-prepared luminescent glyconanospheres. (A) 15 000× image of CdSe-ZnS QDs incorporated in luminescent glyconanospheres. The scale bar is 500 nm. (B) 150 000× high-resolution image of a single luminescent glyconanosphere showing that the glyconanosphere contains many CdSe-ZnS QDs. The scale bar is 50 nm. TEM images are taken using a JEOL 2010 transmission electron microscope. (C) Histogram describing the size distribution of the luminescent glyconanospheres.

in this image. Figure 3.21 (C) shows the size distribution of the luminescent glyconanospheres. Nearly 70% of the glyconanospheres are between 150 and 200 nm in diameter.

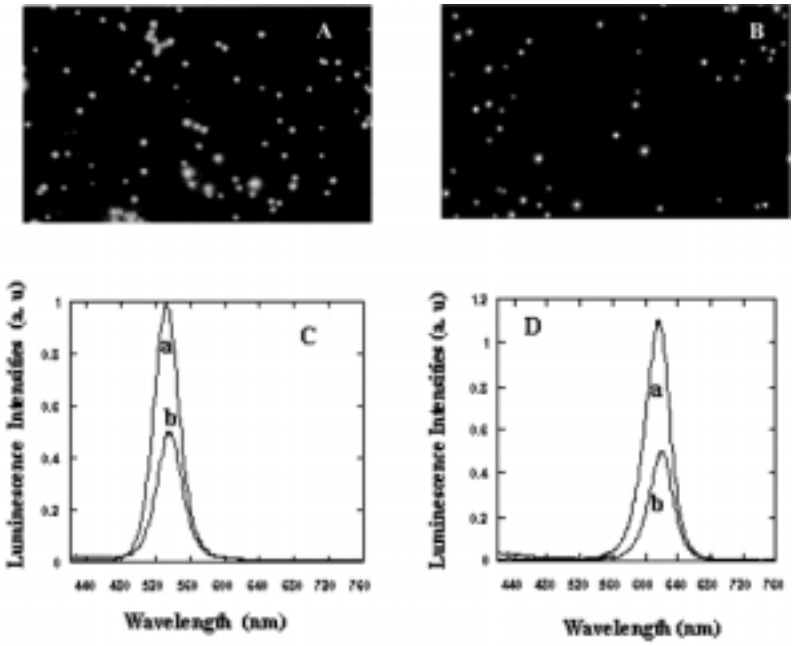

Fig. 3.22 (A) Luminescence image of negatively charged green emission CdSe-ZnS QDs incorporated glyconanospheres. (B) Luminescence image of negatively charged red emission CdSe-ZnS QD incorporated glyconanospheres. (C) Emission spectra of free green emission QDs (curve a) and glyconanospheres containing green emission QDs (curve b). (D) Emission spectra of free red emission QDs (curve a) and glyconanospheres containing red emission QDs (curve b). The luminescence images were taken using a digital fluorescence imaging microscopy system equipped with an intensified charge coupled device camera (ICCD). The excitation wavelength was 470 nm and the magnification of the microscope was 40×. Emission spectra were taken using a Quanta Master PTI fluorometer.

Since this preparation method is based on electrostatic interactions, the size of the QDs should not affect the formation of the nanospheres. Indeed, QDs of different diameter and different emission color were incorporated into the luminescent glyconanospheres. Figures 3.22 (A) and 3.22 (B) show digital luminescence microscopy images of green and red emission QDs containing glyconanospheres. The glyconanospheres are highly luminescent with a signal-to-noise ratio (S/N) of over 100. Figures 3.22 (C) and 3.22 (D) compare between the emission

spectra of solutions containing green and red emission CdSe-ZnS QDs and the spectra of solutions of glyconanospheres incorporating CdSe-ZnS QDs. The emission band of the incorporated QDs is similar to the emission band of free QDs but still shows a 4 nm red shift. This minor red shift may be attributed to a change of surface charge states of the QDs. The intensity differences result from different concentrations of emitting particles and not from a decreased emission quantum yield.

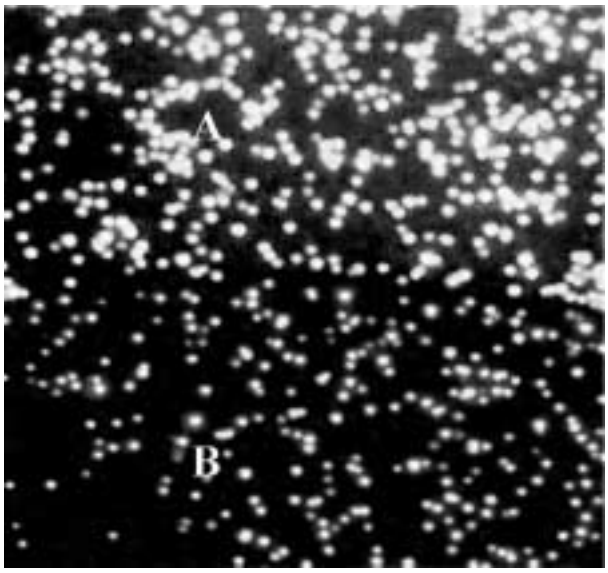

Fig. 3.23 Luminescence images of Oregon green and CdSe-ZnS containing glyconanospheres. The upper half of the image (A) is dominated by the green emission of Oregon Green. The lower half of the image (B) shows the image of the red emission of the glyconanospheres following 3 min irradiation at 470 nm, which effectively bleaches the Oregon Green molecules.

The dextran molecules play an important role in forming the spherical nanospheres and preventing their aggregation. To prove that dextran molecules are indeed incorporated into the

nanospheres, we prepared glyconanospheres with Oregon Green labeled dextran molecules. Oregon-Green is a highly luminescent green dye with fluorescein-like emission properties (λ_{ex} = 470 nm, λ_{em} = 525 nm). It also provides one negative charge for each dye molecule that is attached to the dextran polymeric chain. When excited at 470 nm, the glyconanospheres showed bright green emission due to the emission of Oregon green (Figure 3.23 A). Following illumination of the sample for about 3 min, the emission of the glyconanospheres turned red (the emission color of the QDs) due to rapid photobleaching of the Oregon green molecules (Figure 3.23 B). These experiments confirmed that the dextran molecules are indeed integrated with CdSe-ZnS QDs in the same glyconanospheres.

Unlike the strong attraction of polyelectrolytes often observed in thin films formed on a flat surface using the layer-by-layer deposition technique, we found that electrostatic interactions solely are not strong enough to stabilize the luminescent glyconanospheres. Fluorescence microscopy measurements revealed that these luminescent glyconanospheres dissociated in about 10 h when stored in aqueous solution at room temperature. The relative instability of the electrostatically held glyconanospheres could be attributed to their large surface-to-volume ratio. The interactions of solution ions with surface charges weaken the electrostatic attraction between the positively charged polylysine and the negatively charged CM-dextran, and the mercaptosuccinic acid modified CdSe QDs. To further stabilize the luminescent glyconanospheres, we introduced the standard water-soluble bioconjugate coupling agent 1-ethyl-3-(3)-dimethylaminopropyl carbodiimide (EDC) to initiate the formation of covalent bonds between the carboxylic groups on the surface of the mercaptosuccinic acid modified CdSe QDs and in the CM-dextran chains and the amino groups of the polylysine chains. Figure 3.24 shows the formation pf amide bonds. The concentration of EDC was 500 mM. The reaction mixture

was incubated at room temperature for 2 hours. The sketch shows the formation of cross-linking amide bonds. The formation of amide bonds between the carboxylic and amino groups in the glyconanospheres greatly increased their chemical stability. Luminescence microscopy measurements revealed that the covalently and electro statically held glyconanospheres remained stable for over two months when stored in aqueous solution at room temperature.

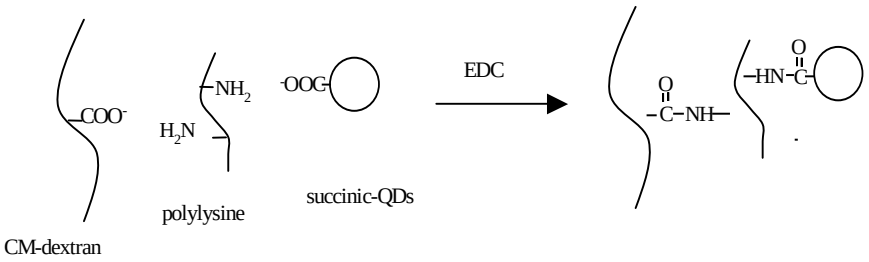

Fig. 3.24. Formation of amide bonds among CM-dextran, poly-L-lysine and succinic capped CdSe-ZnS QDs. The carboxylic groups were activated by EDC.

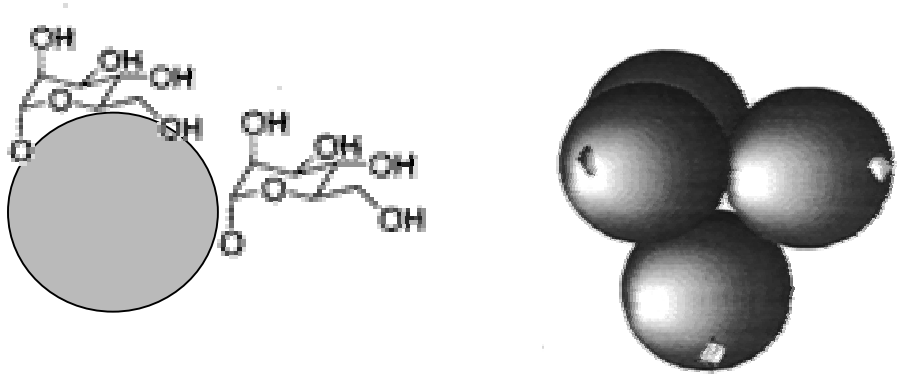

Fig. 3.25. Models of surfaces bound glucose residues and the protein Con A.

CM-dextran provides the glyconanospheres with high surface density of glucosylic residues. Thus, the carbohydrate binding protein concanavalin A (Con A) can recognize the surface bound dextran. The molecular models are shown in figure 3.25. Con A is a lectinic protein that selectively binds to the terminal residues of α-D-glucose and α-D-mannose. Each Con A molecule contains four binding sites for carbohydrates(131). These polyvalent binding sites have been often used in cell agglutination and separation of glycoproteins in affinity chromatography (132). To demonstrate the binding interactions of the surface-bound dextran and Con A, we mixed a solution of 200 μL 0.04 μM (based on the concentration of CdSe-ZnS QDs) glyconanospheres with 2 mL 0.05M HEPES buffer solution (pH 7.2) containing 0.25 mg/mL Con A, 0.1 mM Mn^{2+}, and 0.1 mM Ca^{2+}. The solution was incubated at room temperature for 2 h. As a control, free glucose was added to the solution along with Con A. The aggregation of glyco-nanospheres was prevented by the addition of 15 mg free α-D-glucose. Since glucose molecules effectively competed with the glyconanospheres for the binding sites of Con A. Figure 3.26 (A) shows the fluorescence image of glyconanospheres in the presence of glucose. Figure 3.26 (B) shows the luminescence images of the glyconanospheres following the addition of Con A. Aggregation of the glyconanospheres due to multiple binding with Con A molecules is clearly seen. The aggregation rate depended on the Con A and glyco-nanospheres concentrations.

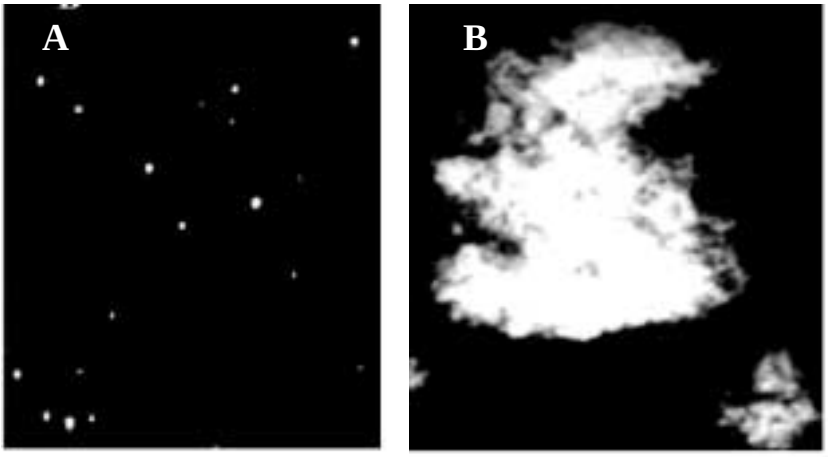

Fig. 3.26 Lectin Con A initiated aggregation of dextran bound CdSe-ZnS QD incorporated luminescent glyconanospheres. (A) Luminescence image of the glyconanospheres in the presence of Con A and free α-D-glucose. The α-D-glucose molecules compete with the glyconanospheres on the Con A binding sites and prevent aggregation. (B) Luminescence image of aggregated glyconanospheres in the presence of Con A.

3.3.1.4 Summary

We have developed a novel method to assemble highly luminescent semiconductor CdSe-ZnS QDs into glyconanospheres through electrostatic interactions and covalent stabilization. The emission properties of the QDs containing glyconanospheres were similar to the emission properties of individual QDs. Assembling hundreds of QDs in single glyco-nanospheres created bright and photostable particles that could be easily observed using conventional fluorescence microscopy instrumentation. This could make luminescent QDs more accessible to fluorescence microscopy studies of biological samples. For example, the luminescent glyconanospheres

showed high affinity to Con A, a glucose specific lectin. As demonstrated in this work, these glyconanospheres could be used to study carbohydrate-protein interactions.

3.3.2 Preparation of Luminescent Semiconductor CdSe-ZnS QDs Doped Stabilized Micelles.

3.3.2.1 Introduction

Surfactant molecules with hydrophobic tails and hydrophilic head groups spontaneously form micelles, lamellar phase or cylindrical rod structures in water when the surfactant concentration is higher than its critical micelle concentration (CMC). The structure, property and concentration of the surfactant molecules determine their morphology when they are dispersed in aqueous solution. A cylindrical rod can further assemble to form a hexagonal structure that has been intensively used as a template to synthesize various mesoporous materials (133-134). This chapter focuses on the application of micelles as carrier for hydrophobic QDs. The hydrophobic core of micelles is a medium that is well-known to solubilize organic dyes according to the "like dissolves like" principle(135-136). Recently, Gao et al. reported using diacyllipid-polymer micelles as nanocarriers to deliver poorly soluble anticancer drugs into cells(137).

However, because surfactant micelles are dynamic species, they undergo dissociation and reformation in the millisecond time scale(138). To overcome this stability problem hydrophilic polymers and organosiloxane shells have been used to stabilize micelles, vesicles, and liposomes(139-140). For example, Katagiri et al. recently synthesized organosilane-functionalized lipid and prepared hybrid organo-inorganic liposomes named cerasomes that averaged 200 nm in diameter. Hydrolysis followed by condensation of the organosilane head

groups of the functionalized lipids led to the formation of a silica layer on the surface of the cerasomes and greatly increased their physical and chemical stability. The cerasomes were used to prepare lipid multilayers using a layer-by-layer assembly technique(141-143). Using a similar principle we developed a novel method to encapsulate lipophilic CdSe QDs in organosilane functionalized surfactant micelles.

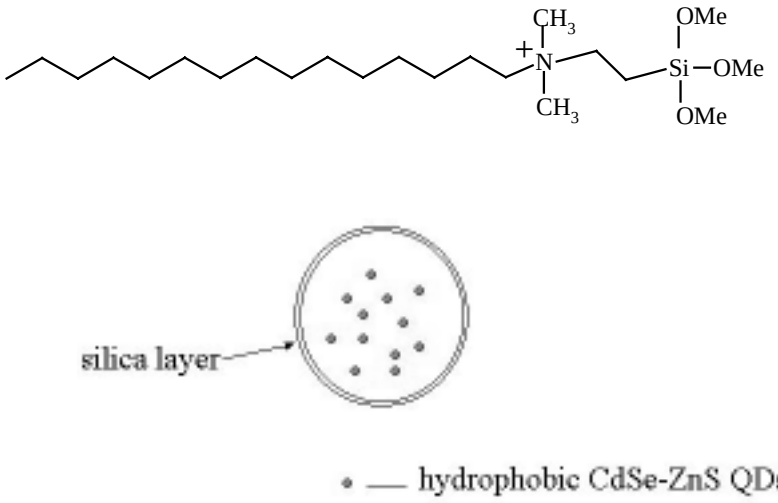

Fig. 3.27. Molecular structure of silane surfactant used in our experiments and the chemical structure of luminescent QDs doped surfactant micelles with a silica layer

A special siloxane surfactant dimethyloctadecyl [3-(trimethoxysilyl) propyl ammonium chloride ($C_{16}H_{33}$-$N^+(Me)_2$-$CH_2CH_2CH_2$-$Si(OMe)_3$ Cl^-) was used to encapsulate lipophilic CdSe QDs. It is a quaternary ammonium surfactant with an organosilane head group (see Figure 3.27). The silane head groups were water sensitive and undergo slow hydrolysis in aqueous solution. The hydrolyzed silane head groups could form cross linking silica shell on the surfaces of

micelles. This chapter describes the synthesis and characterization of the structural, optical and chemical properties of these unique stabilized micelles.

3.3.2.2 Specific experimental details

Materials- cadmium oxide, TOP, TOPO, selenium, diethyl zinc (0.1M solution in heptane), hexamethyldisilanthiane, dimethyloctadecyl [3-(trimethoxysilyl) propyl ammonium chloride, were purchased from Aldrich and used without further purification.

Preparation of green and red emission CdSe QDs- Luminescent CdSe QDs of green emission and red emission colors were synthesized based on a method developed by Peng et al., with minor modifications(49). To prepare green emission QDs, 12 mg CdO and 150 mg lauric acid were loaded in a 100 ml flask, then used septum cap to seal the flask. The flask was flowed with nitrogen for 30 minutes. Then heated to 250 ºC until the red CdO completely dissolved. The solution was cooled to room temperature and loaded 1.5g TOPO and 1.5 g 1-hexadecylamine into the flask. The flask was flowed with nitrogen for another 30 minute. The mixture was heated to 280ºC, then injected 2 ml TOPO solution containing 80 mg Se powder into the hit solution quickly. Then removed the heating mantel and let the solution cooled to 40ºC. The CdSe QDs were precipitated by methanol and collected by centrifuge at 2000 rpm for 5 minutes. Red emission QDs were prepared by using similar procedure except the mixture of Cd-lauric, TOPO and hexadecylamine was heated to 320ºC instead of 280ºC and the heating time was 3 minutes after the injection of Se-TOP solution to facilitate growth of larger nanoparticles.

Preparation of micelles doped with CdSe QDs- To prepare QD-doped micelles, 1 mg CdSe QDs was mixed with a chloroform solution containing the siloxane surfactant

dimethyloctadecyl [3-(trimethoxysilyl) propyl ammonium chloride ($C_{16}H_{33}$-$N^+(Me)_2$-$CH_2CH_2CH_2$-$Si(OMe)_3$ Cl^-). The mixture was then injected drop-by-drop into 10 mL water at 75 °C under magnetic stirring. The elevated temperature was required to evaporate the chloroform. The final concentration of the surfactant in water was as high as 15 mM to ensure the formation of micelles. CdSe QDs were entrapped in the hydrophobic regions of the formed micelles. The formed micelles containing QDs were collected by centrifuge at 3500 rpm for 10 minutes and redispersed in aqueous solution 50 ml deionized water. The pH of the micelle solution was then adjusted to 9.0. The silane head groups were hydrolyzed to form a silica layer on the surface of micelles under these conditions. The micelles solution was then heated to 80˚C for 10 minutes for the condensation of silanol groups to form cross linking silica shell on the surfaces of micelles.

3.3.2.3 Results

Characterization of QDs and micelles doped with QDs- To demonstrate the capability of incorporate different sizes (i.g different emission colors) of QDs in these unique siloxane surfactant micelles. Two different emission colors of green and red QDs were prepared. The QDs were highly luminescent with quantum yield over 50%. The emission maxima of the green and red dots were obtained at 525 nm and 650 nm. Figure 3.28 A and B show transmission electron microscope (TEM) images of green and red emission QDs averaging 3 and 6 nm in diameter, respectively. The particles appear spherical and no aggregation is observed. The image clarity of larger particles is higher due to increased electron density. Trioctylphosphine oxide (TOPO)

ligands on the surface of the CdSe QDs increase their lipophilicity and miscibility in chloroform solutions containing siloxane surfactant.

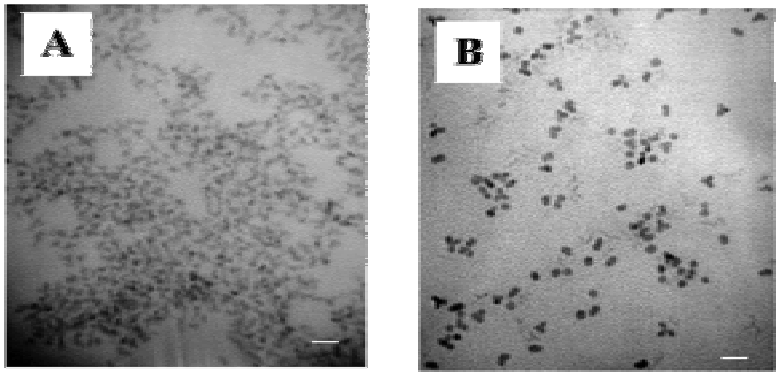

Fig. 3.28 TEM images of free green emission and red emission of QDs in chloroform solution taken on a JOEL 2010 transmission electron microscope. (A) Green emission CdSe QDs averaging 3 nm in diameter. (B) Red emission CdSe QDs averaging 6 nm in diameter. The scale bar is 10 nm.

Figure 3.29 A shows a TEM image of the CdSe QD-doped micelles. The diameter of the micelles ranges from 50 to 130 nm. The wide size distribution is a characteristic of solvent evaporation methods commonly used to prepare micelles or liposomes. Similarly to liposomes, the size distribution could be further narrowed using extrusion techniques. Most of the micelle nanospheres appear to be spherical in shape. However, a small percentage of the micelles appear to have elliptical or irregular shapes. This could be the result of silanol-silanol cross-linking between adjacent micelles. The entrapped QDs make the micelles easily visible in the electron micrographs in contrast to ordinary surfactant micelles that require negative staining for

visualization. A high-resolution TEM image of a CdSe QD-doped micelle is shown in Figure 3.29 B. There are about 300 QDs in this 100 nm micelle.

The lattice structure of the trapped CdSe QDs cannot be defined due to the presence of the surfactant. Most of the encapsulated CdSe QDs are located in the core of the micelle. High-resolution TEM images also reveal that some QD-doped micelles are capped with a silica layer as thick as 12 nm. Because a single layer of cross-linked silica is much thinner than 12 nm, it is reasonable to conclude that multiple layers of surfactant molecules form this thick layer.

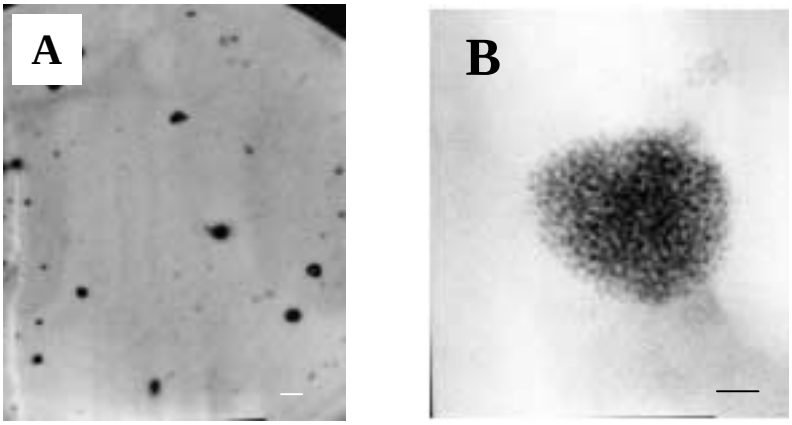

Fig. 3.29. TEM images of CdSe QD-doped micelles. (A) TEM image of QDs doped surfactant micelles ranging from 50 to 130 nm in diameter. The scale bar is 200 nm. (B) HRTEM image of micelles shows that the encapsulated QDs are distributed in the hydrophobic interior of the surfactant micelles. The scale bar is 20 nm

Spectroscopy and microscopy- Because quantum dots were encapsulated in the hydrophobic core of the micelle nanospheres, it was reasonable to expect that the optical properties of the entrapped CdSe QDs would be similar to the optical properties of free CdSe

QDs in chloroform. Figure 3.30 (A) and (B) shows the emission of free QDs in chloroform and encapsulated QDs in our silica capped micelles. The sharp emission spectra and the emission band of both the green emission dots and red emission dots were well preserved following their encapsulation in the micelles. The encapsulated QDs also have similar absorption properties with free QDs in chloroform solution as shown in figure 3.31 (A) and (B). Free QDs of both green and red emission have clear absorption peak at 510 nm and 630 nm respectively. Encapsulated QDs also have absorption peak at these positions. However the absorption peaks of trapped QDs are not sharp due to the influence of surfactant and the scattering of the nanospheres.

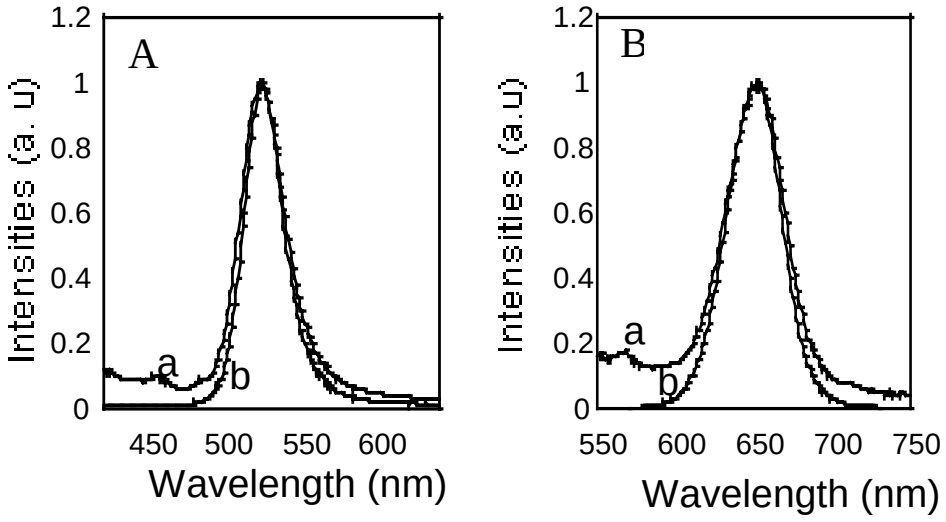

Fig. 3.30 Comparison of emission spectra of free QDs in chloroform solution and encapsulated QDs in micelles. (A) Emission spectra of green emission QDs: (a) free QDs, (b) encapsulated QDs. (B) Emission spectra of red emission QDs: (a) free QDs, (b) encapsulated QDs. Emission spectra were taken with a Quanta Master PTI fluorometer.

Figure 3.32 shows a luminescence image of QD-doped micelles taken using a digital fluorescence imaging microscopy system consisting of an inverted fluorescence microscope equipped with a high performance intensified charge coupled device camera (ICCD). The micelles appear as bright red or green spherical spheres with a signal-to-noise ratio of about 100. By controlling the diameter of the CdSe QDs, we were able to prepare micelles that emit blue, green, yellow, orange, and red light.

Ordinary surfactant molecules such as Areol-OT and CTAB can also be used to encapsulate CdSe QDs to form bright red or green nanospheres in aqueous solution (images not shown). However, these micelles are not stable and are easily destroyed by Alcohol or Triton X-100. The use of the siloxane surfactant facilitates the formation of stabilized micelles due to their capping with a silica layer. In addition to stabilizing the QD-doped micelles, the silica layer provides a large number of chemical derivation sites for conjugation of biomolecules

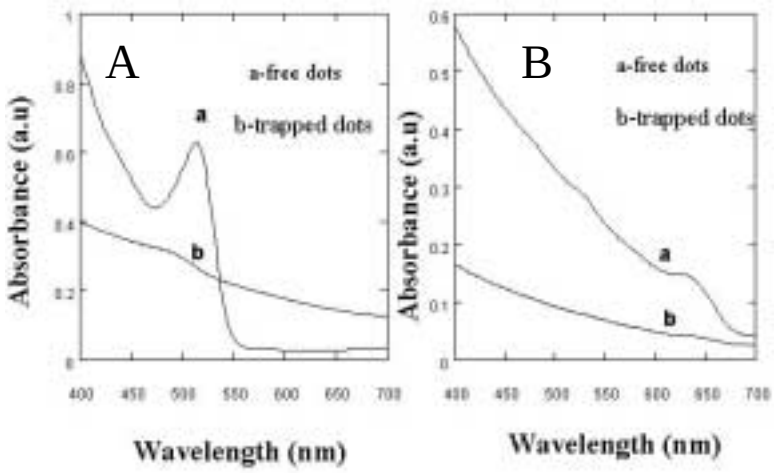

Fig. 3.31 Absorption spectra of free QDs and encapsulated QDs. (A) green emission QDs. curve (a) is free QDs in chloroform solution. curve (b) is encapsulated QDs. (B) red emission QDs. curve (a) is free QDs and curve (b) is encapsulated QDs.

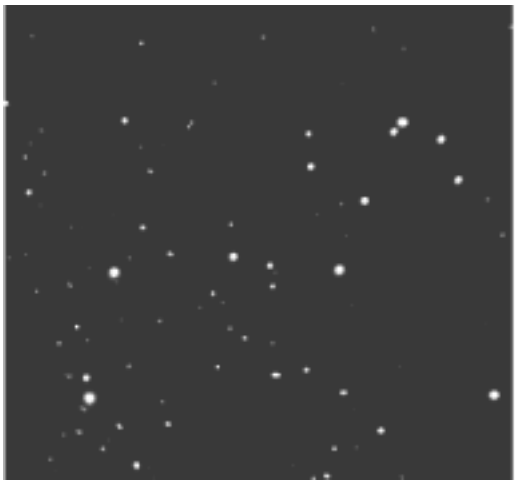

Fig. 3.32. Fluorescence image of QDs doped micelles taken using a digital fluorescence imaging microscopy system equipped with an intensified charge coupled device camera (ICCD). The excitation wavelength was 470 nm and the magnification of the microscope is 40×. The scale bar in the right corner is 400 nm.

3.3.2.4 Summary - a novel method was developed to prepare luminescent CdSe QD-doped micelles coated with a stabilizing silica layer. This method is a general preparation approach that can be used to encapsulate other lipophilic molecules, such as lipophilic organic fluorescent dyes in the micelle nanospheres. The encapsulated QDs maintain their high quantum yield and sharp emission spectra. The silica layer increases the stability of the luminescent micelles compared to micelles formed with AOT and CTAB. The silica layer also makes the surface of micelles accessible to further derivation using standard silane chemistry. These newly developed stable

luminescent micelles could be used as bright fluorescent labels in biological applications involving the conjugation of biomolecules such as enzymes, antibodies, and DNA molecules to the micelles. The advantage of combining multiple QDs in micelles is quite clear. The luminescence intensity of single QDs is low and cannot be observed with sufficient signal-to-background ratio using an ordinary fluorescence microscope. A laser is generally needed to excite the quantum dots. However, the intense laser beam required for excitation of the individual QDs is likely to damage biological samples. The collective emission intensity of a micelle containing hundreds of QDs increases the signal and the signal-to-background ratio considerably without significantly affecting the spatial resolution in the image, as the nanometric size of the micelle is well below the optical limit of diffraction. Doping polymeric particles with luminescent QDs could also lead to similar results obtained by assembling QDs in micelles. Indeed, micrometric polystyrene beads that contain luminescent QDs were successfully developed for multiplex biocoding applications. However, our attempts to prepare nanometric polymer beads doped with luminescent QDs encountered experimental difficulties. Encapsulation of the QDs in nanometric polymer beads affects their morphology. Swelling of the polymer beads in aqueous solution leads to leaking of the QDs into the solution. Additionally, the emission of the QDs is quenched by the polymer and the enhancement in the signal-to-background ratio is not as significant as in QD-doped micelles. The relatively large size distribution of the QD-doped micelles is still a concern. We are currently developing extrusion techniques to narrow the size distribution.

3.3.3 Synthesis and application of Semiconductor CdSe-ZnS QDs Doped Silica Nanospheres (QDSNs) in Bioassay

3.3.3.1 Introduction- Silica based materials are of great interest in preparing nano-composite materials due to their inert chemical properties and optical transparency. Additionally, the chemistry of derivatizing silica nanoparticles on surfaces with a variety of functional groups, such as amino groups ($–NH_2$), and thiol groups (-SH) for conjugation of biomolecules is well established (144-155). Silica has been used to coat different kinds of nanoparticles including gold (146) and magnetic nanoparticles (147). Silica nanospheres were also applied to encapsulate organic dyes for bioanalysis applications (148). Chang et al. (149-150) prepared silica coated CdS QDs with different nanoscale complex morphologies by using a microemulsion based synthetic method. They showed that the CdS QDs could be homogeneously dispersed in silica nanospheres, could be a large inclusion, could be a surface cap or a core of a silica sphere. Kotov et al. (151) used mercptopropyltrimethylsilane derived CdTe QDs as seeds to synthesize CdTe QDs doped silica nanospheres that were about 100nm in diameter. These CdTe QDs doped uniform silica nanospheres could form 3-D colloid crystals for photonic applications.

Although CdS and CdTe QDs have been successfully incorporated into silica nanospheres, these QDSNs only contained a small number of luminescent nanocrystals. Moreover, both CdS and CdTe QDs were synthesized in water pools of a microemulsion or in aqueous solution at room temperature. It was clearly demonstrated that the quantum yield and crystal quality of QDs synthesized in aqueous solution were inferior to that of QDs synthesized in trioctylphosphine

oxide (TOPO) media at elevated temperature. As a result, the QDSNs were not suitable for luminescent biological labeling applications where bright emission is disirable.

This section describes a novel method to incorporate hundreds of highly luminescent CdSe-ZnS QDs inside each individual silica nanosphere. CdSe-ZnS QDs used in our experiment were synthesized in trioctylphosphine oxide (TOPO) media at elevated temperature. The CdSe-ZnS QDs had 50% quantum yield, which is much higher than the quantum yield of QDs synthesized in aqueous solution. The QDSNs were functionalized with the protein streptavidin for conjugation of biotin labeled biomolecules. As an example, biotin labeled protein A was bound to the streptavidin modified QDSNs. These protein A modified QDSNs were used as luminescent indicator in the detection of antiprotein A antibody in a 'sandwich' immunoassay. The detection of antibody was based on counting the number of QDSNs instead of measuring the emission intensity as conducted in conventional fluoroimmunoassays.

3.3.3.2 Specific experimental details

Materials- sodium silicate, oleic acid, thioglycerol, AOT, heptane, streptavidin-maleimide, protein-biotin, anti-protein A, 3-mercaptopropyltrimethoxysilane, 3-aminopropyltrimethoxysilane, N-hydroxysuccinimido-biotin (NHS-biotin), bis(2-ethylhexyl) sulfosuccinate sodium salt (AOT) were obtained from Aldrich and used as received without purification.

Preparation of water soluble CdSe-ZnS QDs- CdSe-ZnS QDs were modified with thioglycerol to transfer the QDs to aqueous solution. The detailed synthesis procedure was described in chapter two.

Preparation of CdSe-ZnS QDs doped silica nanospheres- To prepare QDs doped silica nanospheres, 100 μl 10% sodium silicate and 50 μl 0.2 μM water-soluble QDs were dispersed in 20 ml 0.1 M AOT/heptane solution following sonication in a water bath sonicator until a clear reverse micelles solution was obtained.. 60 μl oleic acid diluted in 2 ml heptane solution was added to the reverse micelle solution to neutralize sodium hydroxide. The solution was stirred for 1 hour. The formed quantum dots doped silica nanospheres were collected by centrifugation at 3000 rpm for 5 minutes, the product was washed 3 times with 10 ml heptane to remove unbounded AOT surfactant.

Functionalization of the luminescent silica nanospheres with thiol groups- The surface of the silica was then functionalized with thiol groups by mixing QDs doped silica nanospheres with 40 μl 3-mercaptopropyltrimethoxysilane in 20 ml 95% ethanol containing 10 μl of 29% ammonia. The solution was stirred at room temperature for 8 hours. The solution was then heated to 70˚C for 5 minutes. The thiol groups modified quantum dots doped silica nanospheres were collected by centrifugation at 3000 rpm for 5 minutes. The silica nanospheres were washed 3 times with ethanol to remove free 3-mercapto-propyltrimethoxysilane.

Synthesis of streptavidin modified QDs doped silica nanospheres- The washed thiol group modified silica nanospheres were dispersed in pH 7.0 phosphate buffer solution following addition of 0.5 mg streptavidin-maleimide. The mixture was incubated at 4˚C for 12 hrs. The streptavidin modified QDs doped silica nanospheres were collected by centrifugation and washed three times with a pH 7.0 phosphate buffer solution. The washed streptavidin functionalized silica nanospheres were dispersed in 2ml phosphate buffer solution and stored at 4˚C.

Binding protein A on the surface of streptavidin modified silica nanospheres- 0.5 mg biotin labeled protein A dissolved in 1ml pH 7.0 phosphate buffer was mixed with 2ml streptavidin modified luminescent silica nanospheres solution for 1 hour at room temperature. Unbounded protein A was removed by centrifugation and wash with pH 7.0 phosphate buffer 3 times. The washed protein A modified luminescent silica nanospheres were dispersed in 3ml pH 7.0 phosphate buffer solution and stored at 4˚C.

Modification of the surface of glass slides with amino groups- glass slides were first cleaned using a 'Piranha' solution which consists of 70% concentrated sulfuric acid and 30% concentrated hydrogen peroxide for 2 hour at 70°C.(caution: 'Piranha' solution is erosive and reacts violently with organic species). The cleaned glass slide was then immersed in a 1% 3-aminopropyltrimethyltrimethylsilciane (APTMS) alcoholic solution overnight to immobilize amino groups on the glass. The amino group functionalized glass slide was rinsed with ethanol solution and annealed at 115°C for 1 hour.

Preparation of protein A modified glass slides- An amino modified glass slide was immersed in a 10 ml of pH7.0 phosphate buffer solution. 20mg N-hydroxylsuccinic biotin (NHS-biotin) was first dissolved in 200 µl DMSO then added to the buffer solution and incubated for 2 hours at room temperature. The slide was rinsed with phosphate buffer sufficiently to remove unreacted biotin. It was then immersed in 10ml pH7.0 phosphate buffer solution that contained 0.4 mg streptavidin. The reaction continued for 1 hour at room temperature. The slide was washed with a pH 7.0 phosphate buffer solution to remove unbound streptavidin. It was then immersed in 10 ml pH 7.0 phosphate buffer solution that contained 0.5mg biotin labeled protein

A for 1 hour. The slides were washed with pH7.0 phosphate buffer solution and stored at 4°C until use.

Detection of anti-protein A- Anti-protein A solution was placed on the surface of a protein A modified glass slide and incubated for two hours at room temperature. Unbound anti-protein A was rinsed with a pH 7.0 phosphate buffer solution. Protein A modified QDs doped silica nanospheres were then added to the glass slide and incubated for two hours at room temperature following rinsing with buffer solution to remove free silica nanospheres. The presence of luminescent silica nanospheres indicated the presence of anti-protein A.

Microscopy and spectroscopy- Fluorescence microscopy images were taken using a digital microscopy system containing a inverted microscope, high performance CCD camera. The image analysis software VinView 3.2 was used for image acquisition and analysis. A JEOL 2010 transmission electron microscope was used to characterize the size and morphology of silica nanospheres doped with QDs.

3.3.3.3 Results

Synthesis of silica nanospheres containing CdSe-ZnS QDs- Reverse micelles were chosen as nanometric reactors to prepare QDs doped silica nanospheres. Reverse micelles are a water-in-oil bi-phase system where nanometer sized water pools (water phase) are dispersed in an organic solvent (oil phase). The water pools are stabilized by surfactant molecules whose hydrophilic head groups point to the water phase and their hydrophobic tail is dissolved in the oil phase. Although CdS and CdTe QDs were successfully encapsulated in silica nanospheres (150-151), the prepared CdS, CdTe QDs doped silica nanospheres were weakly luminescent due to the

low emission efficiency of the encapsulated QDs and the small number of QDs in each silica nanosphere. Inspired by these studies, we used reverse micelles to prepare highly luminescent CdSe-ZnS QDs doped silica nanospheres. The QDs used in our study were CdSe-ZnS QDs with a core shell structure. They were first prepared in TOPO media at elevated temperature; then transferred to aqueous solution.

Previously, Stober et al. (152) developed a novel method to prepare monodisperse silica nanoparticles through the hydrolysis of tetraethyl orthosilicate(TEOS) in alkaline alcohol solution. Since then TEOS has become a silica precursor of choice. Although TEOS was successfully used to synthesize dye doped silica nanospheres in a non-ionic reverse micelles system, we failed to prepare QDs doped silica nanospheres using this method. We therefore replaced TEOS with sodium silicate as silica source in the preparation of the silica nanospheres. Sodium silicate was less expensive than TEOS. It was easily miscible with the water soluble luminescent CdSe-ZnS QDs. Sodium silicate is sensitive to pH. At low pH, the silicate molecules were condensed to silica. We used oleic acid to initiate the formation of silica nanospheres in reverse micelles. Oleic acid itself is an anionic surfactant. Oleic acid neutralized the hydroxylic ions (-OH) in the water phase and caused the condensation of the silicate. Since

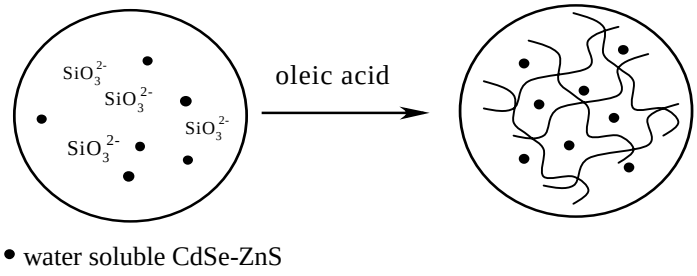

Fig. 3.33 The formation of QDs doped silica nanospheres in the water pool of reverse micelles. The black spots represent water soluble CdSe-ZnS QDs. Addition of oleic acid initiated the condensation of sodium silicate and formed silica cross-linking network where QDs were trapped.

luminescent CdSe-ZnS QDs were mixed with silicate molecules, condensation of silicate trapped the QDs in the silica nanospheres. Figure 3.33 illustrates the trapping of QDs in the silica cross-linked network.

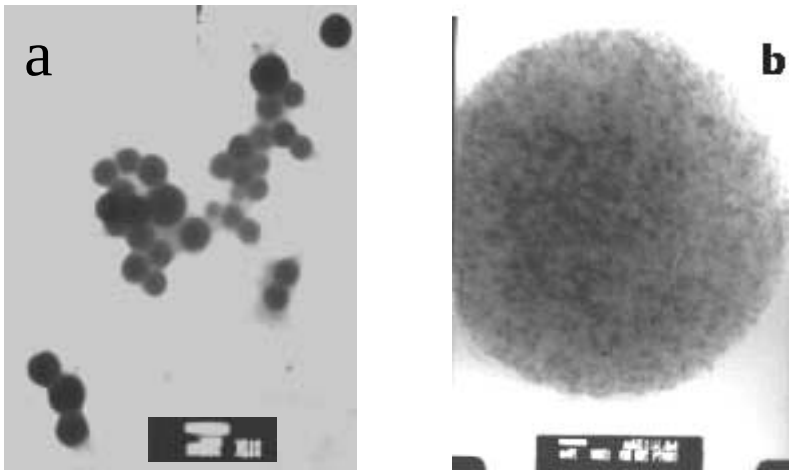

Fig. 3.34 (a) Transmission electron microscope image of CdSe-ZnS QD doped silica nanospheres. The scale bar is 500nm. (b) Enlarged TEM image of a single silica nanospheres doped with QDs. The sale bar is 50 nm. There are hundreds of QDs trapped in the silica nanospheres.

The morphology of the QDs doped silica nanospheres was characterized by TEM as shown in figure 3.34 (a). QDs doped silica nanospheres were not homogeneous in size. Since the size of the water pools in the reverse micelles was not uniform. TEM images revealed that the silica nanospheres were about 180nm in diameter. Figure 3.34 (b) is an enlarged TEM image of a single silica nanosphere doped with QDs. The QDs have higher electron density than silica, thus they appeared to be darker black dots in the sphere. Energy dispersive analysis of X-ray (EDAX)

pattern showed in figure 3.35. The presence of Si, O, Cd, Se, Zn, and S in a QDs doped silica nanosphere confirms that the silica nanospheres contain QDs.

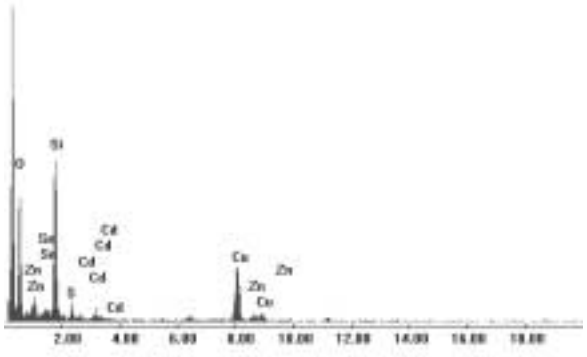

Fig 3.35. An Energy dispersive analysis of X-ray (EDAX) pattern of QDSNs. The elements zinc, cadmium, sulfur and selenium originated from the QDs. The elements silicon and oxygen originated from the silica nanospheres.

When mixing QDs of different emission colors with silicate solution, the QDSNs could be green, yellow and red under irradiation. Figure 3.36 shows a representative image of silica nanospheres that were doped with green, yellow and red emission CdSe-ZnS QDs. As stated earlier, the QDs were synthesized in TOPO media at elevated temperature, thus the silica nanoparticles containing QDs were brightly luminescent under irradiation. The capability to prepare silica nanospheres of multiple emission colors is critical for their successful application in biological samples. Autofluorescence of biological samples often interfere with the analysis.

To eliminate the interference of emission from the sample, it could be possible to choose QDSNs that have a different emission color from that of the analysized biological sample.

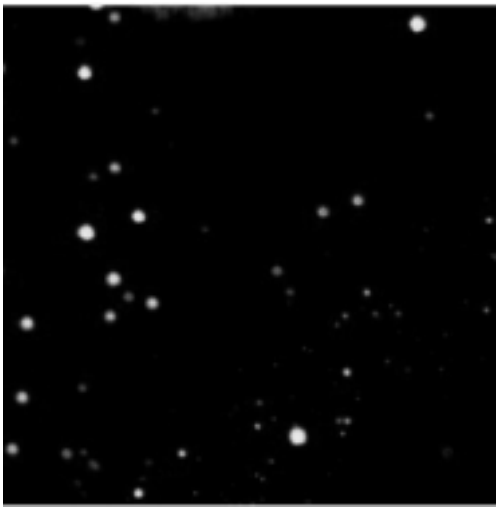

Fig. 3.36 Luminescent image of green, yellow and red emission QDs doped silica nanospheres. The image was taken using a fluorescence microscope with 40X objective. λ_{ex} = 475 nm.

Functionalizing QDs doped silica nanospheres with thiol groups- The QDSNs had no functional groups on the surface. As a result, they could not be conjugated to biological molecules. To overcome this problem, the surface of the QDSNs was grafted with thiol groups through hydrolysis and condensation of 3-mercaptopropyltrimethoxysilane (MPTMS) in a ethanol-ammonia solution. The availability of thiol groups for conjugation of biomolecules was confirmed by monobromobiane (mbbr). mbbr is an organic dye that is weakly fluorescent is solution. When reacting with free thiol groups, the emission intensity of mbbr is greatly

increased. Figure 3.37 shows the fluorescence spectra of mbbr when excited at 380 nm. Curve a is the spectrum of red emission QDSNs without thiol groups. The QDSNs were weakly emission at this region. Curve b was the emission spectrum of mbbr in chloroform solution. Mbbr had low emission at 490nm. After reacting with thiol groups modified QDSNs, the emission intensity of mbbr increased about 4 times (shown in curve c). This result showed clearly that thiol groups were successfully grafted on the surface of QDSNs. Moreover, they were chemically reactive.

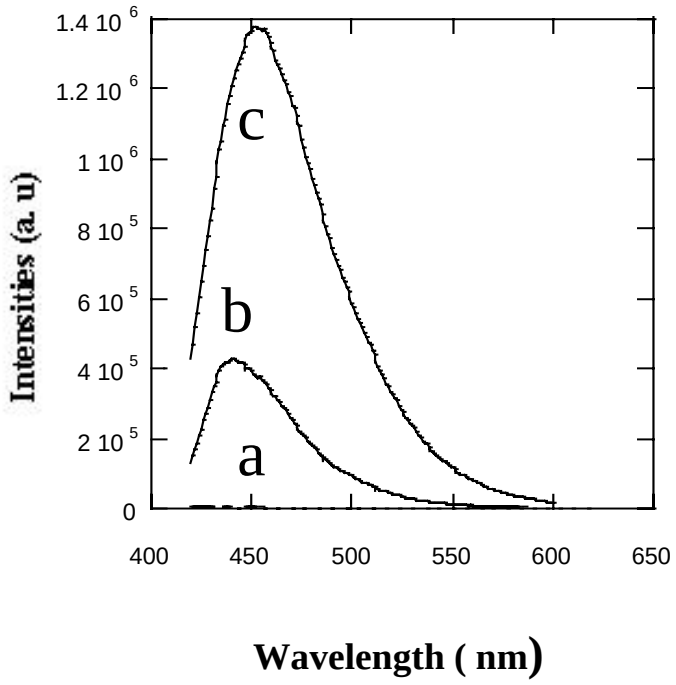

Fig.3.37 Reaction of mbbr and thiol groups modified QDSNs. (a) emission spectrum of thiol modified QDSNs. (b) emission spectrum of mbbr in methanol. (c) emission spectrum of mixture of thiol modified QDSNs and mbbr.

The thiol group was useful in conjugating maleimide labeled streptavidin to QDSNs. Since maleimide could selectively react with thiol groups with high efficiency. The conjugation of streptavidin was illustrated in figure3.38. Streptavidin is a protein that shows specific binding ability to biotin (e.g. vitamin H) through non-covalent bond. The binding constant of streptavidin to biotin is as high as 10^{15} M^{-1} (153). The interaction of streptavidin-biotin has found wide application in analytical chemistry.

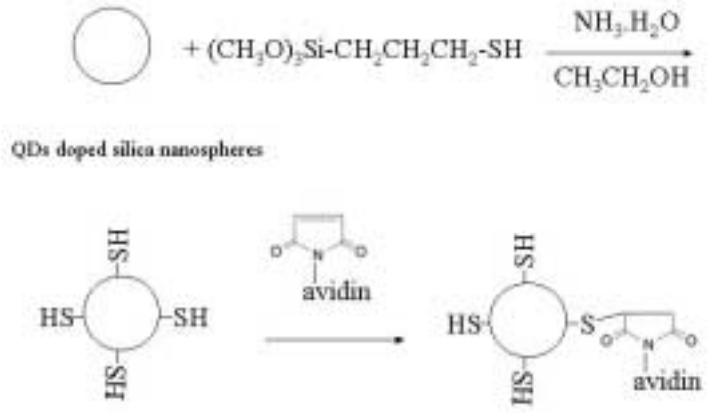

Fig. 3.38 Grafting thiol groups on the surfaces of QDSNs and subsequently conjugating with streptavidin.

To confirm that streptavidin was conjugated on the surface of QDSNs, glass slide modified with biotin was prepared. The procedure to immobilize biotin is shown in figure 3.39. The biotinylated glass slide was then immersed in the streptavidin modified QDSNs solution for 1 hour and rinsed with a pH 7.0 phosphate buffer solution. The glass slide was checked using a fluorescence microscope. Figure 3.40 is the fluorescence image of the glass slide. The presence of many luminescent QDSNs on the glass slide confirmed the success of conjugation of

streptavidin. As a control, QDSNs that were not modified with streptavidin did not show high binding ability to biotin modified glass slide.

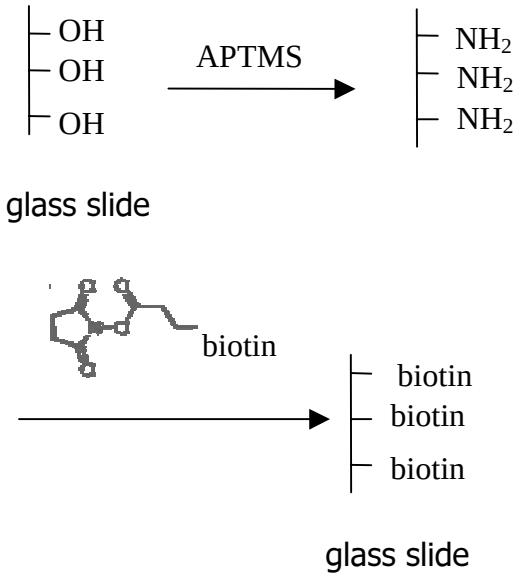

Fig. 3.39 modification of glass slides with biotin.

Fig. 3.40 Image of QDSNs doped with QDs on biotinylated glass slide through streptavidin and biotin interaction. The presence of QDSNs confirmed that streptavidin have been successfully bound on the QDSNs. The image was taken using a 40X objective with a excitation wavelength of 475 nm.

Detection of anti-protein A- To use the streptavidin functionalized QDSNs in bioassay,

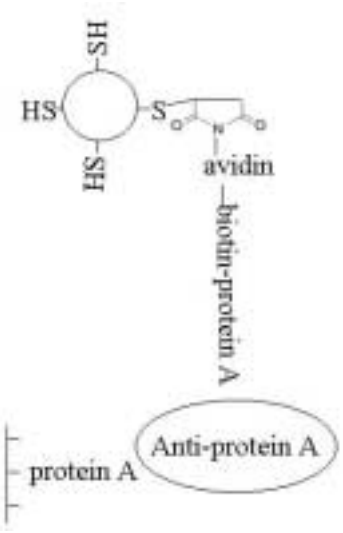

Fig 3.41. Detection of anti-protein A using a 'sandwich type' immunoassay. QDSNs were used to indicate the presence of anti-protein A.

biotin labeled protein A was conjugated to the QDSNs through avidin-biotin interaction. The protein A modified luminescent QDSNs were used as an indicator to detect anti-protein A in a 'sandwich type' immunoassay. In conventional fluoroimmunoassay, the quantification of an analyte was usually based on the measurement of the emission intensity of an organic dye (154-155). In this study, a novel detection strategy was developed to quantify an analyte. As stated previously, the QDSNs was about 180nm in diameter and they were highly luminescent when irradiated with light. Therefore the QDSNs were visible under ordinary fluorescence microscope. The new detection strategy was based on counting the number of the QDSNs that were retained

on glass slide through immunocomplex. Figure 3.41 showed the principle for the detection of a antibody anti-protein A in 'sandwich' immunoassay using QDSNs as a luminescent indicator.

Figure 3.42 are the luminescent images of luminescent QDSNs bound on glass slide at different concentration of anti-protein A. When the solution did not contain anti-protein A, there are a small number of luminescent QDSNs bound on protein A modified glass slide(figure 3.42 a) due to the nonspecific binding that included electrostatic interaction, and hydrophobic interaction. Figure 3.42 (b) and figure 3.42 (c) show the luminescence images of QDSNs when the protein A modified glass slide was immersed in the solution containing antiprotein A antibody at the concentration of 0.01μg/ml and 1μg/ml respectively. These images clearly showed that when immersed in the solution containing different concentration of antibody, the

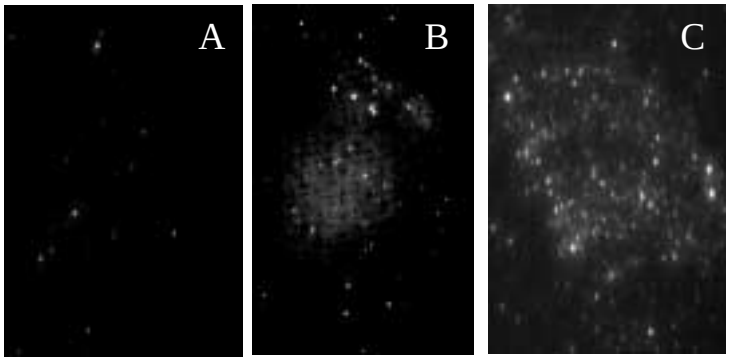

Fig. 3.42 Detection of anti-protein A in a 'sandwich' immunoassay system using QDSNs as indicator. (A) Image of protein A modified QDSNs in the absence of anti-protein A. The presence of a few of protein A-modified QDSNs is due to the non-specific interaction. (B) Image of protein A modified QDSNs at the concentration of 0.01μg/ml anti-protein A. (c) Image of protein A modified QDSNs at the concentration of 1μg/ml anti-protein A antibody.

protein A modified glass slide could retain different number of QDSNs. Higher concentration of antibody retained more luminescent QDSNs. Therefore the antibody concentration of a sample could be determined by counting the number of retained luminescent QDSNs instead of measurement of the emission intensity. Under optimum experimental conditions, this unique immunoassay could reach single molecule detection limit. The presence of one single anti protein A molecule on the glass slide is possible to be detected by QDSNs.

3.3.3.4 Summary- A novel method was developed to assemble highly luminescent semiconductor CdSe-ZnS QDs in silica nanospheres using a reverse micelles system. This synthetic method could be extended for the preparation of silica nanospheres containing other water-soluble nanoparticles. The emission properties of the encapsulated QDs were similar to that of free CdSe-ZnS QDs in aqueous solution. Assembling hundreds of QDs in single nanospheres created bright and photostable particles that were easily observed using ordinary fluorescence microscopy instrumentation. By encapsulating QDs of different emission colors in the silica nanospheres, we prepared green, yellow and red emission QDSNs. These novel QDSNs were modified with streptavidin through a multi-step reaction. Streptavidin provides useful binding sites for conjugation other biotinylated biomolecules through avidin-biotin interaction. As an example, biotin labeled protein A was bound to QDSNs and subsequently they were successfully applied as an indicator to detect anti-protein A. The detection of antiprotein A is based on counting the number of luminescent QDSNs on the glass slide. The detection limit and dection dynamic range will be studied in continuing investigations. These unique highly luminescent QDSNs may find applications in the detection of DNA, protein, bacteria and viruses.

CHAPTER FOUR: SUMMARY AND DISSCUSSION

Luminescent semiconductor QDs have several advantages over organic dyes. For example, sharp and symmetric emission spectra, broad excitation spectra and high photostability. These unique optical properties of QDs attracted great interest. QDs were explored as biological labels and sensors. In this Ph.D study, luminescent semiconductor QDs were successfully synthesized in three different media and Their surface was modified their surfaces with different ligands for ion sensing applications. Three methods were developed to encapsulate both hydrophobic and hydrophilic CdSe QDs into nanospheres including micelles, glyconanospheres and silica nanospheres. The incorporated QDs showed similar optical properties to free QDs in chloroform solution. The glyconanospheres showed binding affinity to a protein Concanavalin A (Con A). Streptavidin modified QDSNs were applied as bright luminescent indicators in an immunoassay for the detection of anti-protein A antibody.

Chapter two includes an overview of the synthetic approaches I used to prepare luminescent semiconductor QDs. The synthesis methods of using reverse micelles, aqueous solution and CdO/TOPO route are discussed. Reverse micelles and aqueous solution routes were simple and easy to handle. However, the quality of QDs prepared using these techniques was generally poor with respect to emission quantum yield and process ability. Although CdSe-CdS QDs synthesized in aqueous solution have 37% emission quantum yield, they did not maintain their optical properties upon surface modification. For example, Modification of the surface of CdSe-CdS QDs with thioglycerol degraded their emission properties. Thioglycerol broadened

emission spectra of QDs. This was attributed to an incomplete CdS shell on the surface of the CdSe cores. Binding of thioglycerol molecules deteriorated the CdS shell and formed many surface defects on the CdSe cores. On the other hand, the CdO/TOPO route produced high quality nanocrystals with over 50% emission quantum yield. Different sizes (i.e different emission colors) of CdSe QDs were synthesized using this method. The growth of a ZnS shell on the surface of CdSe QDs provided the QDs with high stability toward their environment and high process ability. They could endure surface modification without deterioration of their optical properties.

Chapter three discusses the use of QDs as selective ion probes and the methods to encapsulate QDs in nanospheres. The preparation of QDs-based ion selective probes was describe for the first time unique. CdS QDs capped with thioglycerol, cysteine and polyphosphate, the luminescence of CdS QDs responded differently to metal ions. The luminescence of thioglycerol capped QDs was quenched by copper ions while zinc ions and other bivalent metal ions such as calcium, magnesium, cobalt and manganese had only minor effect on the emission of these CdS QDs. On the other hand, the emission of amino acid cysteine capped CdS QDs increased by zinc ions, copper ions and other metal ions had minor effect on the emission of QDs. The emission of polyphosphate capped CdS QDs were easily affected by all tested ions. The reasons for the different response of QDs when exposed to the metal ions are not clearly understood at the present time. Additional experimental information is needed to fully understand this phenomenon. It is clear that metal ions have different abilities to form complexes with certain ligands, such as cysteine. Amino acids usually have higher affinity to zinc ions than to other ions. In this study it was found that zinc ions can cause the aggregation of cysteins

capped CdS QDs through the formation of cysteine-zinc complex. Other ions do not initiate aggregation of CdS QDs. The formation of a complex between cysteine and zinc ions could enhance the emission of CdS QDs through elimination of photo induced electron transfer from the amino group to the valance band of CdS QDs. Elimination of photo induced electron transfer process is the main reason that many organic dyes increase their emission intensities when bind to metal ions. Another possible reason is that some metal ions could undergo a redox reaction with CdS QDs upon irradiation. EPR experiments confirmed that copper ion are reduced by CdS QDs under irradiation. Other ions studied in our experiments such as zinc ions do not have the ability to accept the excited electrons from the conduction bands of CdS QDs. The different chelating ability of surface bound ligands and different redox potentials may cause CdS QDs respond to ions in different ways. However, this is still an active research area, some other groups investigated the use of CdS QDs as sensors for organic molecules and gases. With more information coming out, the understanding of this phenomena will be deepened.

In chapter three a novel and simple route to ensemble hydrophilic CdSe-ZnS QDs into glyconanospheres was also discussed. When CdSe-ZnS QDs modified by mercaptosuccinic acid were mixed with polyelectrolyte polylysine and carboxymethyldextran(CM-dextran), the attraction between positive charges and negative charges led to the formation of luminescent nanospheres that averaged 190nm in diameter. Moreover, the surface bound dextran still kept its biological activity, it could interact with a glucose binding protein Concanavalin A(Con A). This unique luminescent glyco-nanospheres provide luminescent markers for investigation of carbohydrate-protein interactions that are a critical step in bacterial and viral infection by using fluorescence microscopy. Different from layer by layer deposition of polyelectrolytes on flat

surfaces, the stability of glyconanospheres was low and they dissociated within 10 hours after formation. The low stability was due to the high surface to volume ratio of glyconanospheres that enhanced their interaction with solution ionic species. Introduction of covalent amide bonds between the charged precursors improved their stability significantly.

Another novel method was developed to encapsulate lipophilic QDs into micelles. Luminescent semiconductor CdSe QDs that emit light from 520nm(green QDs) to 650nm(red QDs) were trapped into micelles that averaged 150nm in diameter. The encapsulated QDs showed their luminescent properties similar to free QD in chloroform solution. QDs doped micelles showed higher stability than ordinary micelles in which CTAB and AOT are often used as surfactants. The cross-linked silica shell on the surface of our QDs-doped micelles greatly increased their stability. Despite the failure of modifying their surfaces with functional groups, these unique bright luminescent micelles may find application in light emitting devices.

In the last section of chapter three a unique immunoassay sensing method based on QDSNs that were prepared in AOT reverse micelles is described. The sizes of QDSNs averaged 200 nm in diameter. Silica nanospheres usually are synthesized by slow hydrolysis of lipophilic TEOS in reverse micelles or alcoholic solution. The hydrolysis and condensation of TEOS usually takes more than 24 hours. In this study the water-soluble sodium silicate was used as a silica precursor. The formation of silica solid nanospheres in AOT reverse micelles is initiated by oleic acid and completed in minutes. By encapsulating QDs of different sizes, green, yellow and red emission QDSNs were prepared. These QDSNs were highly luminescent and were easily observed with an ordinary fluorescence microscope. Therefore they were suitable for use as luminescent indictors in bioassays. To apply these unique QDSNs in bioassays, their surface was further functionalized with thiol (-SH) groups to enable the conjugation of streptavidin-

maleimide. Streptavidin is a protein that has high binding affinity and high specificity to biotin. As an example, biotinylated protein A was bound on the surface of QDSNs for detecting of antiprotein A antibody in an ‘sandwich’ type immunoassay. Different from conventional immunoassay, the detection of anti-protein A antibody was based on counting the number of absorbed luminescent QDSNs on protein A-anti-protein A immunoplex bound glass slide. Under optimum condition, this detection method can reach single molecule detection limit. These unique highly luminescent QDSNs may be used as biomarkers in protein and DNA assay.

The application of QDs is affected by the lack of synthetic methods that can produce QDs with consistent size and optical properties. QDs prepared using currently available synthesis procedures showed large variation in size and emission bands from batch to batch. A procedure that can repeatedly produce the same size and optical property is valuable for quantitative analysis. More precise control on the surface modification of QDs as well as other nanoparticles needs to be learned. Although a variety of biomolecules have been successfully conjugated on the surface of QDs and other nanomaterials, the accurate number of such biomolecules that were bound on the surface is not clearly known. This limitation prevents such biomolecules modified QDs to provide more quantitative information.

REFERENCES

1. Niemeyer, C. M.; *Angew. Chem .Int. Edit.* **2001,** *40 (22):* 4128-4158.

2. Mirkin, C. A. *MRS Bullitin,* **2000**, 25 (1): 43-54.

3. Pichot, C.; Taniguchi, T.; Delair, T.; Elaissari, A. *J. Disper. Sci . Tech.* **2003**. *24 (3-4)* 423-437.

4. Bell, A. T. *Science* **2003,** *299 (5613):* 1688-1691.

5. Rolison, D. R. *Science.* **2003**, *299 (5613):* 1698-1701.

6. Zhong, C. J.; Maye, M. M. *Adv. Mater***. 2001**, *13 (19):* 1507-1511.

7. Luo, J.; Maye, M. M.; Lou, Y. B.; Han, L.; Hepel, M.; Zhong, C. J. *Catalysis Today***. 2002**. *77 (1-2):* 127-138.

8. Maye, M. M.; Lou, Y. B.; Zhong, C. J. *Langmuir* **2000**. *16 (19):* 7520-7523.

9. Lou, Y.B.; Maye, M. M.; Han, L.; Luo, J.; Zhong, C. J. *Chem. Comm***. 2001.** *(5):* 473-474.

10. Barratt, G. *Cellular and Molecular life Sci***. 2003.** *60 (1):* 21-37.

11. Leroux, J. C.; Allemann, E.; DeJaeghere, F.;Doelker, E.; Gurny, R. *J. Contr. Ralease.* **1996**. *39 (2-3):* 339-350.

12. Brigger, I.; Dubernet, C.; Couvreur, P. Adv. Drug Delivery Rev. 2002. 54 (5): 631-651.

13. Labhasetwar, V.; Song, C. X.; Levy, R. J. *Adv. Drug Delivery Rev***. 1997,** *24 (1):* 63-85.

14. Choi, H.-J.; Johnson, J. C.; He, R.; Lee, S.-K.; Kim, F.; Pauzauskie, P.; Goldberger, J.; Saykally, R. J.; Yang, P.; J. Phys. Chem. B. ; 2003; 107(34); 8721-8725**.**

15. Huang, M.; Mao, S.; Feick, H.; Yan, H.; Wu, Y.; Kind, H.; Weber, E.; Russo, R.; Yang, P. *Science* **2001**, *292(5523)*, 1897-1899.

16. Johnson, J.; Yan, H.; Schaller, R.; Haber, L.; Saykally, R.; Yang, P. *J. Phys. Chem. B* **2001**, *105*, 11387- 11390.

17. Johnson, J.; Choi, H. J.; Knutsen, K. P.; Schaller, R. D.; Saykally, R. J.; Yang, P. *Nat. Mater.* **2002**, *1(2),* 106-110.

18. Banyai, L.; Koch, S. W. *Semiconductor Quantum Dots*. **1993**, World Scientific Singapore.

19. Lubert Stryer. Bichemistry. W. H. Freeman & Company, New York. **1981**, pp1-pp7.

20. Alivisatos, A. P. *Science* **1996,** *271 (5251)*, 933-937.

21. Wang, Y. *Advances in Photochemistry* **1995**, *19*, 179-231.

22. Murphy, C. J. *Anal. Chem*. **2002**, *521* A-525 A.

23. Gaponik, N.; Talapin, D. V.; Rogach, A. L.; Eychmuller, A.; Weller, H.; *Nano Lett.* **2002**; *2(8);* 803-806.

24. Ni, T.; Nagesha, D. K.; Robles, J.; Materer, N. F.; Mussig, S.; Kotov, N. A.; *J. Am. Chem. Soc*. **2002;** *124*(15); 3980-3992.

25. Esumi, K. *Top Curr Chem.* **2003**, *227*, 31-52.

26. Wang, W. L.; Bai, F. L.; Lin, H. Z.; Zhai, *J. Synthetic. Met*. **2003,** *135 (1-3),* 813-814.

27. Matsumoto, H.; Sakata, T.; Mori, H.; Yoneyama, H. *J. Phys. Chem*. **1996**, *100*, 13781-13785.

28. Herron, N.; Wang, Y.; Eckert, H. *J. Am. Chem. Soc*. **1990**, *112*, 1322-1326.

29. Vossmeyer, T.; Katsikas, L.; Giersig, M.; Popovic, I. G.; Diesner, K.; Chemseddine, A.; Eychmuller, A.; Weller, H. *J. Phys. Chem*. **1994**, *98*, 7665-7673.

30. Swayambunathan, V.; Hayes, D.; Schimt, K. H.; Liao, Y. X.; Meisel, D. *J. Am. Chem. Soc*. **1990**, *112*, 3831-3837.

31. Hirai, T.; Bando, Y.; Komasawa, I. *J. Phys. Chem.* B **2002,** *106 (35):* 8967-8970.

32. Hirai, T.; Okubo, H.; Komasawa, I.. *J. Colloid Interf. Sci*. **2001**, *235 (2):* 358-364.

33. Curri, M. L.; Agostiano, A.; Manna, L.; Monica, M.; Catalano, M.; Chiavarone, L.; Spagnolo, V.; Lugara, M. *J. Phys. Chem*. B. **2000,***104 (35)*, 8391-8397.

34. Korgel, B. A.; Monbouquette, H. G. *J. Phys. Chem*. **1996,** *100 (1),* 346-351.

35. Hirai, T.; Watanabe, T.; Komasawa, I. *J. Phys. Chem.* B. **1999**, *103 (46).* 10120-10126.

36. Shiojiri, S.; Hirai, T.; Komasawa, I. *Chem. Commun*. **1998,** *(14)*, 1439-1440.

37. Zang, L.; Shen, T. *Chem Commun*. **1996,** *(4),* 473-474.

38. Towey, T. F.; Khan-Lodhi, A.; Robinson, B. H. J . Chem. Soc. *Farady trans.* **1990**, *86*(22), 3757-3762.

39. Lianos, P.; Thomas, J. K. *Chem. Phys. Letter*. **1986**, *125 (3),* 299-302.

40. Steigerwald, M. L.; Alivisatos, A. P.; Gibson, J. M.; Harris, T. D.; Kortan, R.; Muller, A. J.; Thayer, A. M.; Duncan, T. M.; Douglass, D. C.; Brus, L. E. *J Am. Chem. Soc*. **1988**, *110*, 3046-3050.

41. Do, Y.; Simhon, E. D.; Holm, R. H. *Inorg. Chem*. **1985**, *24*, 1831-1838.

42. Cassagneau, T.; Mallouk, T. E.; Fendler, J. H. *J. Am. Chem. Soc*. **1998**, *120*, 7848-7859.

43. Wang, X.Y.; Qu, L. H.; Zhang, J.Y.; Peng, X. G.; Xiao, M. *Nano Lett.* **2003**, *3 (8)* 1103-1106.

44. Manna, L.; Scher, E. C.; Alivisatos, A. P. *J. Am. Chem. Soc.* **2000**; *122*(51); 12700-12706.

45. Mattoussi, H.; Mauro, J. M.; Goldman, E. R.; Anderson, G. P.; Sundar, V. C.; Mikulec, F. V.; Bawendi, M. G. *J. Am. Chem. Soc.* **2000**; *122*(49); 12142-12150.

46. Mekis, I.; Talapin, D. V.; Kornowski, A.; Haase, M.; Weller, H. *J. Phys. Chem. B.* **2003**; *107*(30); 7454-7462.

47. Talapin, D. V.; Rogach, A. L.; Kornowski, A.; Haase, M.; Weller, H.; *Nano Lett.* **2001**; *1*(4); 207-211.

48. Murray, C. B.; Norris, D. J.; Bawendi, M. G. *J. Am. Chem. Soc*. **1993**, *115*, 8706-8711.

49. Peng, Z. A.; Peng, X.; *J. Am. Chem. Soc.* **2001**; *123*(1); 183-184.

50. Peng, Z. A.; Peng, X. *J. Am. Chem. Soc.* **2001**; *123*(7); 1389-1395.

51. Yu, W. W.; Qu, L.; Guo, W.; Peng, X.; *Chem. Mater*. **2003**; *15*(14); 2854-2860.

52. Pradhan, N.; Efrima, S. *J. Am. Chem. Soc*. **2003**, *125*, 2050-2051.

53. Watzke, H. J.; Fendler, J. H. *J. Phys. Chem.* **1987**, *91*, 854-861.

54. Korgel, B. A.; Monbouquette, H. G. *Langmuir*. **2000**; *16*(8); 3588-3594.

55. Farmer, S. C.; Patten, T. E. *Chem. Mater.* **2001**; *13*(11); 3920-3926.

56. Wang, Y.; Suna, A.; Mahler, W.; Kasowski, R. J. *J. Phys. Chem.* **1987**, *87*, 7315-7322.

57. Mansur, HS, Vasconcelos WL, Grieser F, Caruso F. *J. Mater. Sci.* **1999,** *34 (21):* 5285-5291.

58. Stramel, R. D.; Nakamura, T.; Thomas, J. K. J. Chem. Soc., Faraday, Trans I, 1988, *84*, 1287-1300.

59. Wang, Y.; Herron, N. *J. Phys. Chem*. **1987**, *91*, 257-260.

60. Hayes, D.; Micic, O. I.; Nenadovic, M. T.; Swayambunathan, V.; Meisel, D. *J. Phys*. Chem. **1989**, *93*, 4603.

61. Swayambunathan, V.; Hayes, D.; Schmidt, K. H.; Liao, Y. X.; Meisel, D. *J. Am. Chem. Soc*. **1990**, *112*, 3831-3837.

62. Zelner M, Minti H, Reisfeld R, Cohen H, Tenne R. *Chem. Mater*. **1997,** *9 (11):* 2541-2543.

63. Peng, X.; Schlamp, M. C.; Kadavanich, A.; Alivisatos, A. P. *J. Am. Chem. Soc*. **1997**, *119*, 7019-7029.

64. Hoheisel, W. Colvin, V. L.; Johnson, C. S.; Alivisatos, A. P. *J. Chem. Phys*. **1994**, *101(10)*, 8455-8460.

65. Norris, D. J.; Sacra, A.; Murray, C. B.; Bawendi, M. G. *Phys. Rev. Lett*. **1994**, *72*, 2612-2615.

66. Spanhel, L.; Haase, M.; Weller, H.; Henglein, A. *J. Am. Chem. Soc*. **1987**, *109*, 5649-5655.

67. Hines, M. A.; Guyot-Sionnest, P. *J. Phys. Chem*. **1996**, *100*, 468-471.

68. Dabbousi, B. O.; Rodriguez-Viejo, J.; Mikulec, F. V.; Heine, J. R.; Mattoussi, H.; Ober, R.; Jensen, K. F.; Bawendi, M. G. *J. Phys. Chem*. B **1997**, *101*, 9463-9475.

69. Li, J. J.; Wang, Y. A.; Guo, W.; Keay, J. C.; Mishima, T. D.; Johnson, M. B.; Peng, X.; *J. Am. Chem. Soc*. **2003**, *125*, 12567-12575.

70. Mekis, I.; Talapin, D. V.; Kornowski, A.; Haase, M.; Weller, H. *J. Phys. Chem*. B **2003**, *107*, 7454-7462.

71. Malik, M. A.; O'Brien, P.; Revaprasadu, N. *Chem. Mater*. **2002**, *14*, 2004-2010.

72. Aldana, J.; Wang, Y. A.; Peng, X. *J. Am. Chem. Soc.* **2001**; *123*(36); 8844-8850.

73. Potapova, I.; Mruk, R.; Prehl, S.; Zentel, R.; Basche, T.; Mews, A. *J. Am. Chem. Soc*. **2003**, *125*, 320-321.

74. Wang, Y. A.; Li, J. J.; Chen, H.; Peng, X. *J. Am. Chem. Soc*. **2002**, *124*, 2293-2298.

75. Chan, W. C. W.; Nie, S. *Science* **1998**. *281 (5385):* 2016-2018.

76. Bruchez, M.; Moronne, M.; Gin, P.; Weiss, S.; Alivisatos, A. P. *Science* **1998,** *281 (5385):* 2013-2016.

77. Rosenthal, S. J.; Tomlinson, I.; Adkins, E. M.; Schroeter, S.; Adams, S.; Swafford, L.; McBride, J.; Wang, Y.; DeFelice, L. J.; Blakely, R. D. *J. Am. Chem. Soc*. **2002**, *124(17)* 4586-4594.

78. Akerman, M. E.; Chan, W. C. W.; Laakkonen, P.; Bhatia, S. N.; Ruoslahti, E. *Proc. Natl. Acad. Soc*. **2002**, *99(20)* 12617-12621.

79. Larson, D. R.; Zipfel, W. R.; Williams, R. M.; Clark, S. W.; Bruchez, M. P.; Wise, F. W.; Webb, W. W. *Science*, **2003**, *300(5624):* 1434-1436.

80. Dubertret, B.; Skourides, P.; Norris, D. J.; Noireaux, V.; Brivanlou, A. H.; Libchaber, A. *Science* **2002,** *298(5599):* 1759-1762.

81. Wu, X.; Liu, H.; Liu, J.; Haley, K. N.; Treadway, J. A.; Larson, J. P.; Ge, N.; Peale, F.; Bruchez, M. P. *Nature Biotechnol*. **2003**, *21*, 41-46.

82. Goldman, E. R.; Anderson, G. P.; Tran, P. T.; Mattoussi, H.; Charles, P. T.; Mauro, J. M. *Anal. Chem*. **2002**, *74(4);* 841-847.

83. Goldman, E. R.; Balighian, E. D.; Mattoussi, H.; Kuno, M. K.; Mauro, J. M.; Tran, P. T.; Anderson, G. P. *J. Am. Chem. Soc.* **2002**; *124*(22); 6378-6382.

84. Han, M. Y.; Gao, X. H.; Su, J. Z.; Nie, S. *Nature Biotech*. **2001**, *19(7):* 631-635.

85. Tian, Y.; Newton, T.; Kotov, N.; Guldi, D. M.; Fendler, J. H. *J. Phys. Chem*. **1996**, *100*, 8927-8939.

86. Ramsden, J. J.; Gratzel, M. J. Chem. Soc. *Faraday Trans*. I, **1984**, *80*, 919-922.

87. Hao, E.; Sun, H.; Zhou, Z.; Liu, J.; Yang, B.; Shen, J. *Chem. Mater.* **1999**; *11(11);* 3096-3102.

88. Spanhel, L.; Weller, H.; Fojtik, A.; Henglein, A. Ber, Bunsenges. Phys. Chem. **1987**, *91*, 88-92.

89. Henglein, A. *Topics in Current Chem*. **1988**, *143*, 113-179.

90. Gerion, D.; Pinaud, F.; Williams, S. C.; Parak, W. J.; Zanchet, D.; Weiss, S.; Alivisatos, A. P. *J. Phys. Chem. B.* **2001**; *105(37);* 8861-8871.

91. Peng, X. G.; Wilson, T. E.; Alivisatos, A. P.; Schultz, P. G. *Angew. Chem., Int. Ed. Engl*. 1**997**, *36*, 145-147.

92. Peng, X.; Wickham, J.; Alivisatos, A. P. *J. Am. Chem. Soc*. **1998**, *120 (21),* 5343-5344.

93. Qu, L.; Peng, X. *J. Am. Chem. Soc*. **2002**, *124 (9),* 2049-2055.

94. Qu, L.; Peng, Z. A.; Peng, X. *Nano Lett*. **2001**, *1 (6),* 333-337.

95. Myung, N.; Bae, Y.; Bard, A. J. *Nano Lett.***2003**; *3(6);* 747-749.

96. Reiss, P.; Bleuse, J.; Pron, A. *Nano Lett.***2002**; *2(7);* 781-784.

97. Sooklal, K.; Cullum, B. S.; Angel, S. M.; Murphy, C. J. *J. Phys. Chem*. **1996**, *100(11),* 4551-4555.

98. Moore, D. E.; Patel, K. *Langmuir* **2001**, *17*, 2541-2544.

99. Gao, M.; Kirstein, S.; Mohwald, H.; Rogach, A.; Kornowski, A.; EychmÜller, A.; Weller, H. *J. Phys. Chem*. B **1998**, *102*, 8360-8363.

100. Diaz, D.; Robles, J.; Ni, T.; Castillo-Blum, S.; Nagesha, D.; Alvarez-Fregoso, O.; Kotov, N. *J. Phys. Chem*. B **1999**, *103*, 9859-9866.

101. Lakowicz, J.; Gryczynski, I.; Gryczynski, Z.; Murphy, C. *J. Phys. Chem*. B **1999**, *103*, 7613-7620.

102. Landes, C.; Burda, C.; Braun, M.; El-Sayed, M. A. *J. Phys. Chem*. B **2001**, *105*, 2981-2986.

103. Landes, C.; Braun, M.; El-Sayed, M. A. *J. Phys. Chem*. B **2001**, *105*, 10554-10558.

104. Horvath, O. *Langmuir* **1999**, *15*, 279-281.

105. Bavykin, D. V.; Savinov, E. N.; Parmon, V. N. *Langmuir* **1999**, *15*, 4722-4727.

106. Isarov, A.; Chrysochoos, J. *Langmuir* **1997**, *13*, 3142-3149.

107. Henglein, A. *Chem. Rev*. **1989**, *89*, 1861-1873.

108. Ramsden, J. J.; Webber, S. E.; Gratzel, M. *J. Phys. Chem*. **1983**, *87*, 474-478.

109. Prodi, L.; Bollrtta, F.; Montalti, M.; Zaccheroni, N. *Helv. Chim. Acta* **2001**, *84*, 609-706.

110. Hennrich, G.; Walther, W.; Resch-Genger, U.; Sonnenschein, H. *Inorg. Chem*. **2001**, *40*, 641-644.

111. Bargossi, C.; Fiorini, M. C.; Montalti, M.; Prodi, L.; Zaccheroni, N. Coord. *Chem. Rev*. **2000**, *208*, 17-32.

112. Klein, G.; Kaufmann, D.; Schuch, S.; Reymond, J.-L.; *Chem. Commun*. **2001**, 561-562.

113. Imperiali, B.; Perace, D. A.; Sohna, J.-E.; Walkup, G.; Torrado, A. *Adv. Mat. Opt. Syst. Chem. Biol. Detect.* **1999**, *3585,* 135-143.

114. Torrado, A.; Walkup, G. K.; Imperiali, B. *J. Am. Chem. Soc*. **1998**, *120 (3),* 609-610.

115. Yang, C.; Awschalom, D.; Stucky, G. *Chem. Mater*. **2001**, *13*, 594-598.

116. Brey, W. Physical Chemistry and Its Biological Applications; Academic Press, New York, **1978**.

117. Canzoniero, L.; Turetsky, D.; Choi, D. *J. Neurosci*. **1999**, *19 (19),* RC31/1-RC31/6.

118. Sensi, S.; Canzoniero, L.; Yu, S.; Ying, H.; Koh, J.; Kerchner, G.; Choi, D. *J. Neurosci*. **1997**, *17 (24),* 9554-9564.

119. Dumitrascu, G.; Kumbhar, A.; Zhou, W.; Rosenzweig, Z. *Trans. Magn*. **2001**, *37 (4),* 2932-2934.

120. Barbara-Guillem, E. US 2002001716 A, **2001**.

121. Rogach, A. L.; Nagesha, D.; Ostrander, J. W.; Giersig, M.; Kotov, N. A. *Chem. Mater*. **2000**, *12,* 2676-2685.

122. Moffitt, M.; Vali, H.; Eisenberg, A. *Chem. Mater*. **1998**, *10,* 1021-1028.

123. Decher, G.; Hong, J. D.; Schmitt, J. *Thin Solid Films* **1992**, *210(1-2),* 831-835.

124. Decher, G.; Hong, J. D. *Makromol. Chem. Macromol. Symp*. **1991**, *46,* 321-327.

125. Anzai, J.; Hoshi, T.; Nakamura, N.; *Langmuir* **2000**, *16(15),* 6306-6311.

126. Caruso, F.; Trau, D.; Mohwald, H.; Renneberg, R.; *Langmui*r **2000**, *16(4),* 1485-1488.

127. Pathak, S.; Choi, S.-K.; Arnheim, N.; Thompson, M. E. *J. Am. Chem. Soc*. **2001**, *123(17),* 4103-4104.

128. Willard, D. M.; Carillo, L. L.; Jung, J.; Van Orden, A. *Nano Lett*. **2001**, *1(9),* 469-474.

129. Rebizak, R.; Schaefer, M.; Dellacherie, E. *Bioconjugate Chem*. **1997**, *8(4),* 605-610.

130. Striolo, A.; Ward, J.; Prausnitz, J. M.; Parak, W. J.; Zanchet, D.; Gerion, D.; Milliron, D.; Alivisatos, A. P. *J. Phys. Chem*. B **2002**, *106(21),* 5500-5505.

131. Ballerstadt, R.; Schultz, J. S. *Anal. Chem*. **2000**, *72(17),* 4185-4192.

132. Lis, H.; Sharon, N. *Chem. Rev*. **1998**, *98(2),* 637-674.

133. Lei, C.; Shin, Y.; Liu, J.; Ackerman, E. J.; *J. Am. Chem. Soc*. **2002**; *124(38);* 11242-11243.

134. Boissiere, C.; Martines, M. A. U.; Kooyman, P. J.; de Kruijff, T. R.; Larbot, A.; Prouzet, E.; *Chem. Mater.* **2003**; *15(2);* 460-463.

135. Riegelman, S.; Allawala, N. A.; Hrenoff, M. K.; Strait, L. A. *J. Colloid Sci.* **1958**, *13*, 208-217.

136. Eriksson, J. C.; Gillberg, G. *Surf. Chem*. **1965**, 148-156.

137. Gao, Z.; Lukyanov, A. N.; Singhal, A.; Torchilin, V. P. *Nano Lett*. **2002**, *2(9),* 979-982.

138. Fendler, J. C.; Fendler, E. J. Catalysis in Micellar and Macromolecular Systems; Academic Press: New York, **1975**.

139. Kawakami, K.; Nishihara, Y.; Hirano, K. *J. Phys. Chem*. B **2001**, *105,* 2374-2385.

140. Ishiwatari, T.; Shimizu, I.; Mitsuishi, M. *Chem. Lett*. **1996**, 33-34.

141. Katagiri, K.; Ariga, K.; Kikuchi, J. *Chem. Lett*. **1999**, 661-662.

142. Katagiri, K.; Hamasaki, R.; Ariga, K.; Kikuchi, J. *J. Am. Chem. Soc*. **2002**, *124(27),* 7892-7893.

143. Katagiri, K.; Hamasaki, R.; Ariga, K.; Kikuchi, J. *Langmuir* **2002**, *18(17)*, 6709-6711.

144. Beaudet, L.; Hossain, K. Z.; Mercier, L. *Chem. Mater*. **2003,***15 (1):* 327-334.

145. Deng, G.; Markowitz, M. A.; Kust, P. R.; Gaber, B. P. *Mat. Sci. Eng C-Bio S* **2000**, *11* (2): 165-172.

146. Graf, C.; Vossen, D. L. J.; Imhof, A.; van Blaaderen, A.; *Langmuir*. **2003**; *19*(17); 6693-6700.

147. Zhao, X.; Tapec-Dytioco, R.; Wang, K.; Tan, W.; *Anal. Chem.* **2003**; *75*(14); 3476-3483.

148. Zhao, X.; Tapec-Dytioco, R.; Tan, W.; *J. Am. Chem. Soc.* **2003**; *125*(38); 11474-11475.

149. Song-yuan Chang, Lei Liu, and Sanford A. Asher. *J. Am. Chem. Soc*. **1994**, *116*, 6739-6744.

150. Song-yuan Chang, Lei Liu, and Sanford A. Asher. *J. Am. Chem. Soc*. **1994**, *116*, 6745-6747.

151. Rogach, A. L.; Nagesha, D.; Ostrander, J. W.; Giersig, M.; Kotov, N. A.; *Chem. Mater*. **2000**; *12(*9); 2676-2685.

152. Stober, W.; Fink, A.; Bohn, E. *J. Colloid Interface Sci*. 1968, *26*, 62-69.

153. Wilchek M, Bayer EA. *Anal Biochem*. **1988,**5; *171*(1):1-32.

154. Schobel, U.; Coille, I.; Brecht, A.; Steinwand, M.; Gauglitz, G.; *Anal. Chem.* **2001**; *73*(21); 5172-5179.

155. Schobel, U.; Egelhaaf, H.-J.; Brecht, A.; Oelkrug, D.; Gauglitz, G.; Bioconjugate Chem. 1999; *10*(6); 1107-1114.

APPENDIX

Glossary of Terms

QDs: Quantum Dots.

TOP: Trioctylphosphine

TOPO: Trioctylphosphine Oxide

$(TMS)_2S$: Hexamethyldisilanthiane

MUA: 11-Mercaptoundecanoic acid

$Zn(Et)_2$: Diethyl Zinc

TSQ: N-(6-methoxy-8-quinolyl)-p-toluenesulfonamide

Con A: Concanavalin A

CM-Dextran: Carboxymethyl Dextran

EDC:1-ethyl-3-(3)-dimethylaminopropyl carbodiimide

AOT: Bis(2-ethylhexyl) sulfosuccinate sodium salt

CTAB: Hexadecyltrimethylammonium bromide

APTMS: 3-Aminopropyltriethoxysilane

MPTMS: 3-Mercaptopropyltrimethoxysilane

TEOS: Tetraethyl Orthosilicate

Mbbr: Monobromobiane

XRD: X-ray diffraction

TEM: Transmission electron microscope.

VITA

The author was born in Anhui, China. He obtained his Bachelor's degree in biochemical engineering from Eastchina Institute of Chemical Technology in 1989. After worked in a pharmaceutical firm for two years, he went back to school and entered the graduate school of Eastchina Institute of Chemical Technology. In 1994 he got the M. S degree in chemistry. He taught inorganic chemistry in Shanghai Jiao Tong University from 1994 to 1999. In 1999, he joined the chemistry department of the University of New Orleans.